The Bakhuis ultrahigh-temperature granulite belt (Suriname): I. petrological and geochronological evidence for a counterclockwise P-T path at 2.07-2.05 Ga

Emond W.F. de ROEVER (1)
Jean-Michel LAFON (2)
Claude DELOR (3)
Alain COCHERIE (3)
Philippe ROSSI (3)
Catherine GUERROT (3)
Alain POTREL (4)

La ceinture de granulites d'ultra-haute température des Monts Bakhuis (Suriname) : I. mise en évidence d'un chemin P-T anti-horaire à 2,07-2,05 Ga

Abstract

The Bakhuis belt, one of the major granulite-facies domains in the Guiana Shield, consists of a core of banded rocks of the charnockite suite, metamorphosed and migmatized under granulite-facies conditions. Pelitic gneiss intercalations locally show sapphirine-quartz and orthopyroxene-sillimanite-quartz assemblages, with up to 10% Al_2O_3 in the orthopyroxene. These assemblages point to ultrahigh-temperature (UHT) metamorphism. P-T conditions are difficult to deduce, because the assemblages contain Fe^{3+} in sapphirine and sillimanite, and do not contain coeval garnet, but spinel, Fe- and Fe-Ti oxides instead. P-T conditions for the peak UHT metamorphism are estimated to have been 950 °C and 8.5-9 kb. An assemblage of impure corundum associated with quartz may also have formed during the UHT metamorphism. Unravelling the assemblages indicates a counterclockwise P-T path from an early cordierite-sillimanite assemblage via a subsequent sapphirine-quartz assemblage to the peak metamorphic assemblage orthopyroxene-sillimanite-quartz. Retrogressive assemblages show an isobaric to near isobaric cooling path for the UHT occurrence.

Single zircon Pb-evaporation and whole rock Sm-Nd dating were carried out on the Bakhuis granulites. Three zircons from a garnet-sillimanite-bearing gneiss yielded an age of 2072 ± 4 Ma, but a fourth grain provided increasing ages up to 2.10 Ga. An enderbitic granulite gave zircon ages in the range of 2.15-2.09 Ga. Zircons from a garnet-bearing gneiss defined an age of 2055 ± 3 Ma, while those from a garnet-bearing pegmatite layer gave ages ranging between 2085 Ma and 2058 Ma. A mylonitic orthopyroxene-bearing granite (a true charnockite) furnished a Pb-Pb zircon age of 2065 ± 2 Ma - this is the first indication that the high-grade metamorphism was (at least locally) associated with melting and production of magmatic charnockite. Zircons from two samples of a discordant recrystallized basic dyke yielded ages of 2060 ± 4 Ma and 2056 ± 4 Ma, respectively. A discordant sheared pegmatite vein provided an age of 2059 ± 3 Ma. In conclusion, the 2072–2055 Ma ages are interpreted as the age of granulite metamorphism in the Bakhuis Mountains, and ages older than 2.07 Ga, and up to 2.15 Ga, are considered to reflect an inherited component from the early Transamazonian protoliths of the granulite.

T_{DM} model ages for the Bakhuis samples range from 2.40 to 2.19 Ga. These data, together with positive to slightly

(1) ONDEO Nalco Europe, Leiden, P.O. Box 627, 2300 AP Leiden, The Netherlands. E-mail: ederoever@nalco.com.
(2) Pará-Iso, Centro de Geociências, UFPA, Belém, Brazil.
(3) brgm, 3, avenue Claude-Guillemin, BP 6009, 45060 Orléans cedex 2, France.
(4) Earth Sciences department, Memorial University of Newfoundland, Canada.

negative $\varepsilon_{Nd(t)}$ values (+1.43 to -0.37), strongly suggest a short crustal-residence time. The isotopic investigations thus demonstrate that the high-grade metamorphism in the Bakhuis belt occurred at 2072-2055 Ma, without significant Archean inheritance.

Monazite appears, for the U-Th-Pb system, to be a reservoir as robust as zircon, as shown by monazite ages which are older than the high-grade metamorphism, 2127 Ma for a garnet-sillimanite gneiss and 2103 Ma for a leucogranite layer. In addition, monazite from the leucogranite layer also registered a much younger thermal event around 2007 Ma, which probably corresponds to the magmatic pulse at about 1.98 Ga recorded by zircon from an anorthosite. Surprisingly, the U-Th-Pb system of the monazite in the two samples did not record the high-grade metamorphic event.

The UHT metamorphism in the Bakhuis belt occurred rather late in the Transamazonian thermo-tectonic continuum. We suggest that the exceptional P-T conditions of the UHT metamorphism in the Bakhuis belt, its counterclockwise P-T path and the simultaneous production of magmatic charnockite are best interpreted as the result of late Transamazonian mantle upwelling, of which ubiquitous metadolerite dykes represent contemporaneous pulses, and younger anorthosite and gabbroic-ultramafic bodies later pulses.

Résumé

La ceinture des Monts Bakhuis, l'un des domaines granulitiques majeurs du bouclier guyanais, constitue un noyau de charnockites litées, métamorphosées et migmatitisées en faciès granulite. Les intercalations de gneiss pélitiques présentent localement des assemblages minéralogiques à sapphirine-quartz et à orthopyroxene-sillimanite-quartz, avec une teneur en Al_2O_3 atteignant jusqu'à 10 % dans l'orthopyroxène. Ces assemblages traduisent un métamorphisme de type ultra-haute température (UHT). Les conditions P-T sont difficiles à déduire dans ces assemblages, de par la teneur en Fe^{3+} dans la sapphirine et la sillimanite, et de par l'absence de grenat et la présence de spinelle et d'oxydes ferrotitanés. Les conditions P-T du climax métamorphique sont estimées à 950 °C et 8,5-9 kb. Un assemblage à corindon impur et quartz se rapporte peut-être aussi au métamorphisme UHT. Le décryptage de ces assemblages minéralogiques permet de conclure à un chemin P-T antihoraire, depuis un assemblage cordierite-sillimanite vers un assemblage intermédiaire sapphirine-quartz jusqu'à un assemblage orthopyroxène-sillimanite-quartz, au pic du métamorphisme. Des assemblages rétrogrades montrent un refroidissement isobare des paragenèses UHT.

Des datations par la méthode Pb-évaporation sur zircon et par la méthode Sm-Nd sur roche totale sont présentées pour les granulites des Monts Bakhuis. Pour un gneiss à grenat-sillimanite, un âge à 2072 ± 4 Ma a été obtenu sur 3 zircons mais un quatrième grain a donné des âges atteignant 2.10 Ga. Une granulite enderbitique a donné des âges zircons dans la fourchette 2.15-2.09 Ga. Un gneiss à grenat a fourni un âge de 2055 ± 3 Ma tandis qu'une intercalation de pegmatite à grenat a donné des âges entre 2085 Ma et 2058 Ma. Un granite à orthopyroxène, à faciès mylonitique (une charnockite sensu stricto) a donné un âge Pb-Pb sur zircon de 2065 ± 2 Ma. Cette observation constitue la première évidence que le métamorphisme de haut grade était (au moins localement) associé avec des processus de fusion et à la production de magmas charnockitiques. Les zircons extraits de deux échantillons d'un dyke basique discordant et recristallisé ont donné des âges à 2060 ± 4 Ma et 2056 ± 4 Ma, respectivement. Une veine pegmatitique discordante et déformée a fourni un âge de 2059 ± 3 Ma. Les âges à 2072-2055 Ma sont interprétés comme l'âge du métamorphisme granulitique des Monts Bakhuis, les âges plus vieux que 2.07 Ga et jusqu'à 2.15 Ga étant considérés comme hérités de protolithes éo-transamazoniens pour ces granulites.

Les âges modèles T_{DM} des échantillons des Monts Bakhuis variant entre 2.40 Ga et 2.19 Ga pour des valeurs de $\varepsilon_{Nd(t)}$ comprises entre +1.43 et -0.37, suggèrent fortement une courte période de résidence crustale pour les protolithes des granulites. Ces résultats isotopiques démontrent que le métamorphisme de haut degré dans les Monts Bakhuis s'est déroulé vers 2072-2055 Ma, sans héritage archéen significatif.

La monazite se révèle être, pour le système U-Th-Pb, un chronomètre aussi robuste que le zircon, comme l'attestent les âges les plus vieux obtenus sur monazites d'un gneiss à grenat-sillimanite (2127 Ma) et d'une intercalation leucogranitique (2103 Ma). D'un autre côté, les monazites de cette intercalation ont enregistré un évènement thermique bien plus jeune daté à 2007 Ma, à relier probablement à une pulsation magmatique datée à 1.98 Ga par les zircons d'une anorthosite. De façon inattendue, dans les deux échantillons, le système U-Th-Pb de la monazite ne semble pas avoir enregistré l'évènement métamorphique de haut degré.

L'âge du métamorphisme UHT dans les Monts Bakhuis est assez tardif au sein du continuum thermo-tectonique transamazonien. Nous suggérons que les conditions P-T exceptionnelles du métamorphisme UHT des Monts Bakhuis, son chemin P-T antihoraire et la production simultanée de magmas charnockitiques sont interprétables comme le résultat de diapirs mantelliques tardi-transamazoniens, dont les manifestations synchrones apparaissent sous forme de dykes omniprésents de métadolérite, et de générations plus tardives d'anorthosites ainsi que de gabbros et de termes ultrabasiques.

Introduction

Granulite belts of modern and ancient orogenies are nowadays considered to be of critical importance for characterizing the geodynamic driving forces involved. Collisional, extensional and strike-slip contexts have been documented for the belts from their Pressure-Temperature-Time paths and from their structural relationships with adjoining terrains.

In the Guiana Shield, which makes up the northern part of the Amazon Craton, high-grade metamorphic domains have been reported in the Imataca Complex (Venezuela), in the Kanuku Mountains (Guyana), in the Bakhuis Mountains and Coeroeni area (Suriname), and in eastern Amapá (Brazil). During the preparation of the Geological Map of Suriname in the 1970s, de Roever (1973, 1975; de Roever *et al.*, 1976) discovered the presence of sapphirine and surinamite in quartz-bearing rocks from the Bakhuis Mountains and found evidence for exceptionally high conditions of metamorphism. Reductions within the Surinam Geological and Mining Service, as well as other factors, prevented a more detailed study of these high-grade assemblages. Moreover, deciphering the P-T history was difficult at the time due to the lack of precise thermobarometric data, while the low sensitivity of the isotopic methods and the large error on age determinations (± 50-100 Ma) precluded any attempt to establish a refined timing of metamorphic events relative to other metamorphic domains of the Shield.

Petrological and experimental studies for determining P-T conditions of granulitic metamorphism have been considerably refined over the last two decades, allowing more accurate interpretations of observed mineral assemblages. Furthermore, occurrences of ultrahigh-temperature (UHT) metamorphism, at 900-1100 °C, have been documented as a special subdivision within the granulite facies (e.g. Harley, 1998). They have been found, in particular, in Archean and Proterozoic terranes where the lowest crustal levels are exposed.

Meanwhile, the development of the Pb-evaporation method on zircon (Kober, 1986, 1987) has proven to be a powerful dating tool, not only allowing precise age determinations on single grains and showing old inherited Pb components in younger rocks, but also enabling magmatic ages to be determined in metamorphic rocks (Jaeckel *et al.*, 1997; Kouamelan *et al.*, 1997; Bartlett *et al.*, 1998), even if it has led to some uncertainties on the crystallization age of rocks with a complex geological history. Whole rock Nd model-age determination has now been established as a tool for finding the protolith age, even in granulite-facies rocks where the zircons may have been partly or completely reset during metamorphism.

The use of these new petrological and isotopic tools has enabled us to present a Pressure-Temperature history of the Bakhuis granulite belt, with detailed descriptions of its exceptional UHT conditions of metamorphism, its P-T path and its isotopic constraints. The geodynamic implications of the Pressure-Temperature history of the belt at the scale of the Guiana Shield are discussed in a companion paper (Delor *et al.*, 2003).

Geological setting

Since the pioneering work of Gibbs and Barron (1993), compilations of the Guiana Shield have been improved 1) by Tassinari (1996), Tassinari and Macambira (1999), and Tassinari *et al.* (2000) and 2) by Santos *et al.* (2000) (see Fig. 1A, 1B), with a special focus on contrasting global ages of crustal accretion, i.e. the reworking of earlier protoliths and the formation of newly juvenile crust.

Archean protoliths have been documented in the far western Imataca Complex in Venezuela (e.g. Montgomery and Hurley, 1978; Tassinari *et al.*, 2001) and the far eastern Amapá belt in Brazil (e.g. João and Marinho, 1982; Montalvão and Tassinari, 1984; Lafon *et al.*, 1998; Avelar *et al.*, 2003). Between these two areas, the Proterozoic crust shows evidence of younging crustal growth (Tassinari *et al.*, 2000; Santos *et al.*, 2000) from a northern Paleoproterozoic granite-greenstone complex (2.2 - 2.0 Ga) to southern zones of acid volcanism (1.9 - 1.8 Ga), sedimentary basin deposition (1.8 - 1.7 Ga) and alkaline magmatism (1.7 - 1.3 Ga). The dominant northern Paleoproterozoic formations, often referred to as the "Maroni-Itacaiúnas" province (see Tassinari *et al.*, 2000), form the major part of the Guiana Shield and essentially comprise greenstone belts and plutonic complexes emplaced during the so-called Transamazonian orogeny - the major tectonothermal event between 2.2 and 2.0 Ga. The present Guiana Shield architecture is mainly the result of these Precambrian geodynamic events. Phanerozoic formations (sediments and dykes), where observed, give an account of the subsequent continental break-up during the Paleozoic (Amazon Basin) and the Mesozoic (Atlantic margin).

Granulite-facies domains have been identified in a) the Imataca belt to the west, b) the Amapá terrain to the east, and c) the Central Guyana belt in the middle.

The Imataca belt, a northeast-trending horst zone in the northwestern corner of the Guiana Shield, contains both granulite-facies and amphibolite-facies rocks (Dougan, 1974). The granulite-facies rocks are mainly felsic granulite (quartz + K-feldspar + plagioclase + orthopyroxene + biotite) with slight foliation, and subordinate intermediate and mafic granulite (two pyroxenes + hornblende + biotite). Metasediments include iron formation (quartz + magnetite ± orthopyroxene), manganiferous quartzite, and pelitic rocks (with widespread cordierite, garnet, sillimanite, biotite, orthopyroxene and Fe-Ti oxides) (Dougan, 1974).
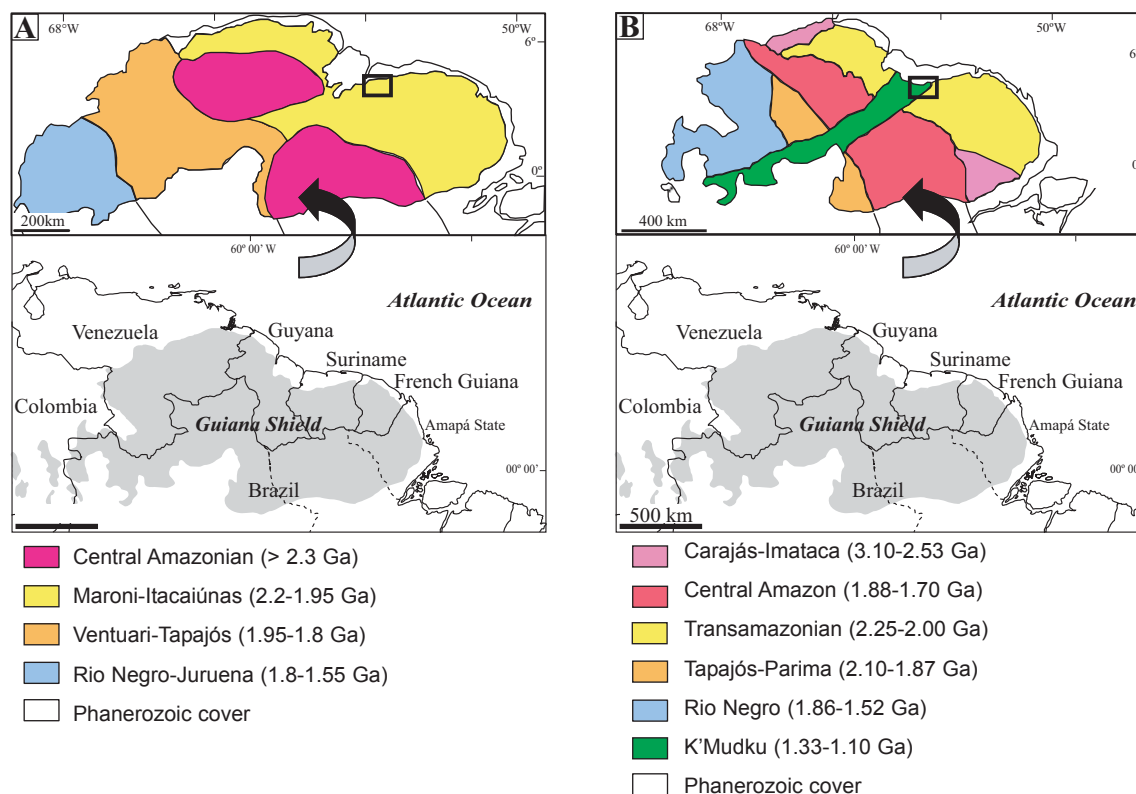
Fig. 1.- Sketch maps of the Guiana Shield according to A) Tassinari *et al.* (2000), and B) Santos *et al.* (2000).

Fig. 1.- *Schémas structuraux du Bouclier Guyanais selon A) Tassinari* et al. *(2000), et B) Santos* et al. *(2000).*

The bulk of the complex consists of felsic granulite or gneiss of uncertain origin and with a fairly homogeneous appearance. Clear metasediments and compositional banding are only of minor importance. The belt has been interpreted as a series of mainly acid igneous rocks, with minor extrusive and sedimentary rocks.

U-Pb, Rb-Sr and Sm-Nd dating of the metamorphic and igneous rocks points to a complex Archean/ Paleoproterozoic history (Montgomery, 1979; Montgomery and Hurley, 1978; Teixeira *et al.*, 1999; Tassinari *et al.*, 2001). The granulite-facies metamorphism was first considered to be Transamazonian, at around 2.1 Ga (Montgomery and Hurley, 1978), but a later study (Tassinari *et al.*, 2001) tended to indicate an Archean granulite-facies event in the core of the Imataca Complex, followed by Transamazonian high-grade resetting on its southeastern margin. The Cerro Bolivar gneiss (with cordierite-sillimanite assemblages) in the southwest of the Imataca Complex, has been dated at 2.32 – 2.19 Ga (Tassinari *et al.*, 2001, and pers. comm.), testifying to Transamazonian high-grade metamorphism.

In central and southern Amapá, the limits of the granulitic domain are as yet poorly delineated. Two-pyroxene-bearing assemblages are found (João and Marinho, 1982; Lafon *et al.*, 2001; Avelar, 2002; Rosa-Costa *et al.*, 2003). The age of the granulitic event is still uncertain. João and Marinho (1982) suggested an Archean age for the event based on a Rb-Sr age of 2.45 Ga; this age, however, probably refers to the protolith without providing the age of the metamorphism itself. Charnockitic intrusions have been dated at 2.05 Ga and 2.06 Ga by U-Pb on zircon (Avelar *et al.*, 2001; Lafon *et al.*, 2001), and Oliveira *et al.* (2002) obtained Sm-Nd ages around 2.03 - 2.0 Ga on metamorphic minerals from surrounding granulitic gneiss. In southeastern Amapá and northwestern Pará, Pb-Pb geochronological results on zircon from granulitic gneiss and charnockitic magmatic rocks suggest an Archean age for the high-grade episode, but Transamazonian ages have also been obtained (Ricci *et al.*, 2002; Rosa-Costa *et al.*, 2003). As in Imataca, the existence of two high-grade metamorphic events, an Archean one and a Transamazonian one, cannot be ruled out.

The "Central Guyana Granulite belt" (Kroonenberg, 1975, 1976) stretches from western Suriname across southern Guyana (Kanuku Horst) into the State of Roraima in Brazil. As originally proposed, the belt would have two branches in Suriname: a NE branch comprising the Bakhuis horst and a SE branch in the Coeroeni area in southwestern Suriname. The word "belt" is misleading (Gibbs and Barron, 1993). Aeromagnetic evidence (Hood and Tyl, 1973) and lack of relief E of the Kanuku horst do not support a straight continuation in the direction of the Bakhuis horst, but a southeastward continuation to the Coeroeni area. In

Suriname the Bakhuis belt disappears towards the southwest below partially mylonitized biotite granite, leucogranite and metavolcanics, in part as a result of its domal structure. The Kanuku horst also appears to have a domal structure (Berrange, 1977; Gibbs and Barron, 1993). Rb-Sr whole-rock dating of the Coeroeni gneiss from drill cores and river samples gave an age of 2001 ± 97 Ma (Priem *et al.*, 1977), whereas Rb-Sr whole-rock dating of Kanuku gneiss and granulite samples gave an age of 2052 ± 50 Ma (Spooner *et al.*, 1971).

The Kanuku complex in Guyana consists of migmatite, predominant paragneiss, and granulite (Berrange, 1977). The paragneiss shows compositional banding, isoclinal folding and widespread migmatization. The Kanuku granulite is structurally distinct from the paragneiss in its lack of gneissic layering and compositional banding (Berrange, op. cit.). Mappable granulite bodies are discordant, fairly homogeneous and uniform, and have the shape of small structural domes. Parts of the granulite have a medium-grained hypidiomorphic-granular fabric, in some cases with megacrysts. Field relationships suggest that at least part of the granulite massifs represent bodies of tonalitic rock intruded into the paragneiss under granulite-facies conditions (Gibbs and Barron, 1993).

The Coeroeni gneiss in southwestern Suriname comprises a predominantly sedimentary series; mainly quartzofeldspathic gneiss and sillimanite gneiss, with minor amphibolite (Kroonenberg, 1976), metamorphosed in the amphibolite or granulite facies. It commonly shows intense folding and migmatization. The structure of the Coeroeni area suggests a migmatite massif intruded in a highly mobile state, with a granulite-facies core (Kroonenberg, 1976).

The Bakhuis belt in northwestern Suriname comprises the high-grade metamorphic rocks of the Falawatra Group, mainly banded rocks of the charnockite suite and pelitic gneiss and locally areas with banded amphibolite and gneiss (de Roever, 1973). The belt occurs in a northeast-trending horst, which coincides with a highly anomalous magnetic zone. Long, mylonitized faults separate the horst and its high-grade rocks from Transamazonian granite, leucogranite and metavolcanics, and some low-grade metamorphic rocks. Horst formation and mylonitization occurred during the Nickerie metamorphic episode at about 1.2 Ga (Priem *et al.*, 1971; this is called the K'Mudku event in Guyana (Snelling and McConnell, 1969). The 1.2 Ga age has been retained as the dominant age for the Bakhuis belt in the compilation map of the Guiana Shield by Santos *et al.* (2000).

The Bakhuis belt

The Bakhuis belt takes a special place among the granulite-facies domains of the Guiana Shield. In the first place, an Archean age for the protolith has not been proven, contrary to the Imataca and Amapá domains, and the high-grade metamorphism is considered to be of Transamazonian age (Priem *et al.*, 1978; Bosma *et al.*, 1983). In the second place it has a central position in the Shield, contrary to the external Imataca and Amapá domains. Last, but not least, the high-grade metamorphism in the Bakhuis Mountains is exceptional; migmatization occurred under granulite-facies conditions, as shown by orthopyroxene-bearing leucosomes (de Roever, 1973). Furthermore, orthopyroxene-sillimanite-quartz and sapphirine-quartz assemblages have been reported by de Roever (1973, 1975) and de Roever *et al.* (1976). These assemblages are typical of ultrahigh-temperature (UHT) metamorphism.

The UHT assemblages are fairly rare and occur amidst rather "ordinary" granulite-facies rocks. Therefore, the latter rocks will be described first to show the context for the UHT metamorphism, followed by a description of the UHT occurrences. Although the amount of available microprobe analyses is still limited and few assemblages were suitable for geothermobarometry, we shall attempt to estimate the P-T conditions and reconstruct the P-T path of the UHT metamorphism.

Granulite-facies metamorphism in the Bakhuis Mountains

Lithological characteristics

The central part of the Bakhuis horst (Fig. 2) consists almost entirely of a zone, 30-40 km wide by 100 km long, of banded rocks of the charnockite suite. Detailed descriptions are given by de Roever (1973, 1975), Dahlberg (1973) and Bosma *et al.* (1978, 1983). These rocks show a conspicuous, neat and ubiquitous compositional banding at centimetre to metre scale (Fig. 3), with foliation of both mafic and felsic minerals, and a mainly granoblastic texture. The rocks almost invariably contain orthopyroxene. Leucoenderbite and enderbite predominate, followed by norite, pyroxene amphibolite and leuconorite (see Appendix, note 1, for nomenclature used); acid rocks are less common. The conspicuous and fairly regular character of the compositional banding suggests a predominantly metasedimentary (and/or metavolcanic) nature. This is also indicated by intercalations of clear metasediments, such as pelitic gneiss, sillimanite quartzite, spessartine quartzite (gondite), calc-silicate rock (calcite-scapolite quartzite), and graphite-bearing (enderbitic) bands. Pelitic gneiss forms intercalations and narrow mappable lenses in the banded rocks of the charnockite suite.

At macroscopic scale, the banding is enhanced by small-scale, incipient migmatization, with thin, parallel leucosomes. Veins cutting across mafic bands and across folds are also common. The leucosomes and veins have a granoblastic texture, and are most commonly composed of coarse-grained leucoenderbite, with some coarse orthopyroxene as only mafic mineral.
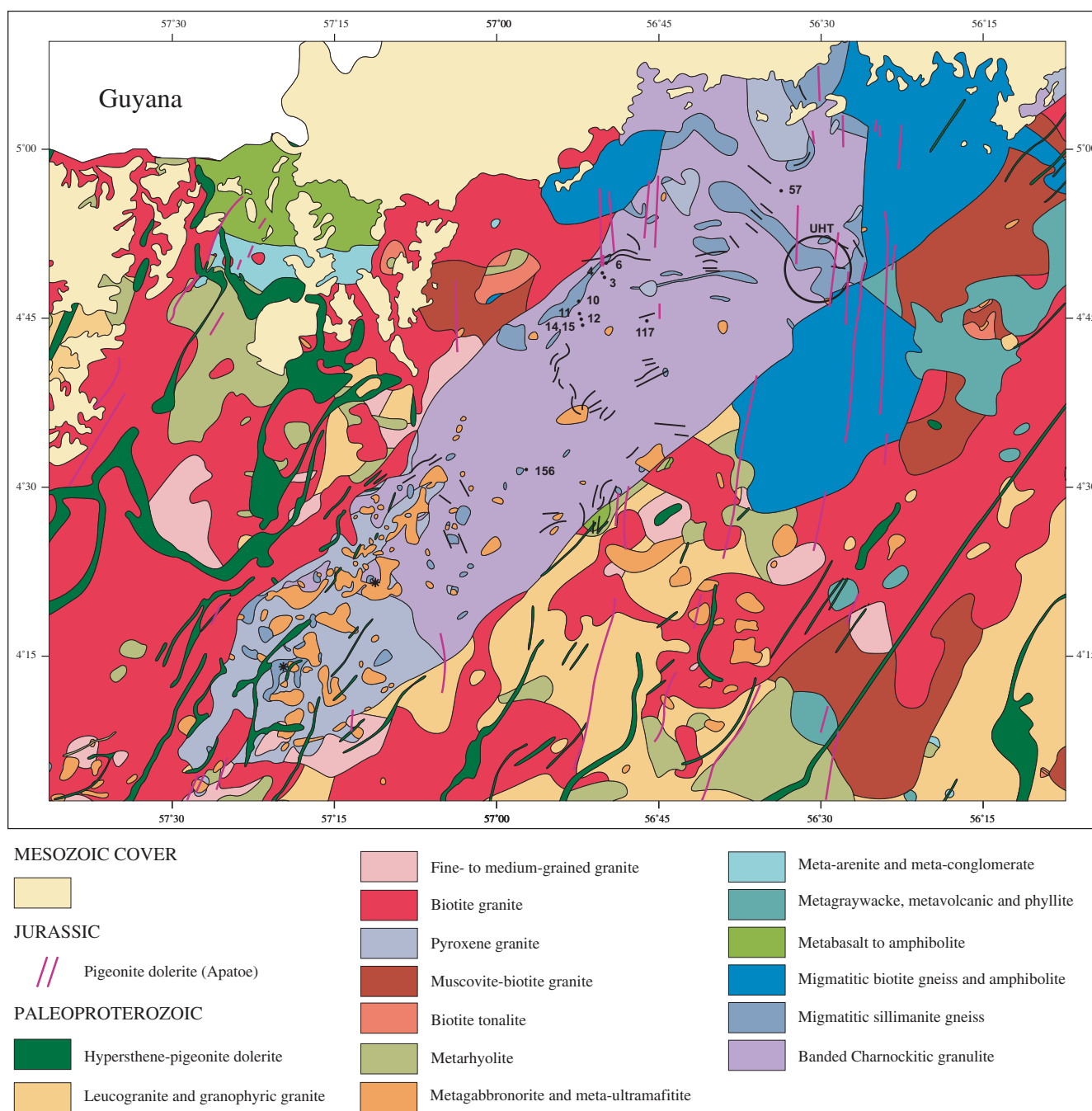
Fig. 2.- Geological map of the Bakhuis granulite belt in NW Suriname, after Bosma *et al.*, 1978 (slightly simplified). The locations of the analysed geochronological samples are indicated (3-15 refer to Su 3-15, 57 to LC-57, 117 to ER 117 and 156 to LA 156). The UHT occurrence in the northeastern part of the belt is shown by a circle, and the two possible UHT remnants in the southwestern part by asterisks. Thin black lines indicate the strike of foliation.

Fig. 2.- Carte géologique de la ceinture granulitique des Bakhuis à l'ouest du Suriname, selon Bosma et al.*, 1978 (simplifié légèrement). La localisation des échantillons analysés en géochronologie y est indiquée (3-15 se réfère à Su 3-15, 57 à LC-57, 117 à ER 117 et 156 à LA 156). La zone UHT dans la partie nord-est de la ceinture est indiquée par un cercle, et les deux reliques UHT possibles au sud-ouest par des astérisques. Le figuré de fines lignes noires représentent les trajectoires de foliation.*

The banded rocks commonly show isoclinal or tight folding, with steeply dipping fold axes (Fig. 3). Basic bands show boudinage, with patches of leucoenderbite between boudins. Discordant or partly deformed metadolerite (pyroxene amphibolite) dykes are quite common.

Metamorphic assemblages

The banded rocks of the charnockite suite consist essentially of orthopyroxene + plagioclase ± clinopyroxene ± hornblende ± biotite ± quartz ± K-feldspar, with accessory magnetite, ilmenite and apatite. The plagioclase
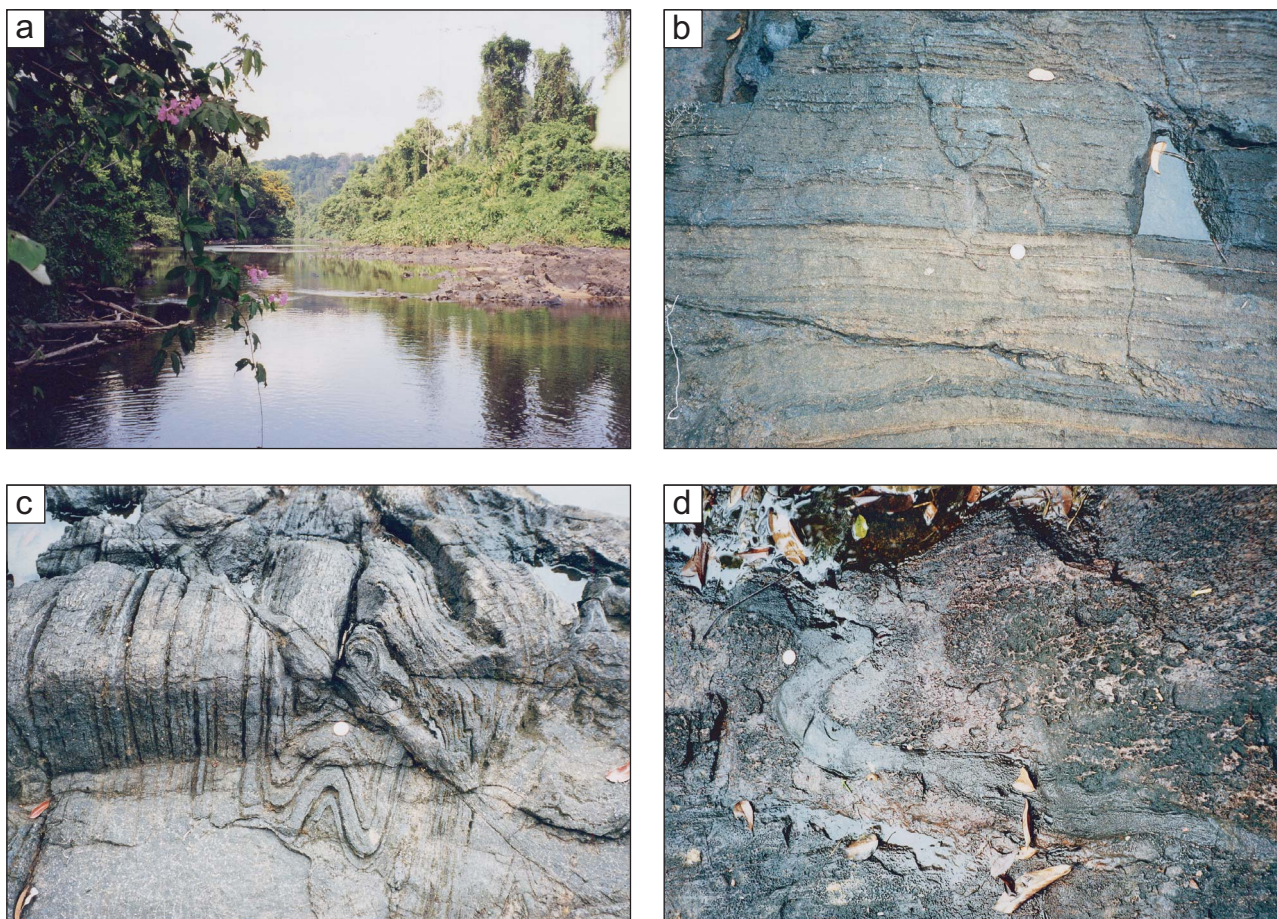
Fig. 3.- Field photographs of the banded rocks of the charnockite suite, showing a) typical outcrop, b) banding, c) folding, d) discordant synkinematic metadolerite dyke. Good outcrops occur mainly along rivers and small streams.

Fig. 3.- Photographies de terrain de la suite de charnockites litées, montrant a) un affleurement caractéristique, b) le litage, c) des plis, d) un dyke de métadolérite syntectonique discordant. Les bons affleurements sont localisés principalement le long des rivières et des petits cours d'eau.

is antiperthitic, and the K-feldspar perthitic or mesoperthitic. The occurrence of orthopyroxene points to granulite-facies metamorphism. However, orthopyroxene is not restricted to mafic compositions, but also occurs widely in quartz-bearing, intermediate and acid rocks. Moreover, migmatization also occurred under granulite-facies conditions, as indicated by the common presence of orthopyroxene in the leucosomes and cross-cutting veins. The isoclinal or tight folding, accompanied by foliation of the rocks, was synkinematic with the metamorphism.

Coeval garnet, indicative of medium-pressure granulite-facies conditions, is typically lacking. Signs of typical UHT metamorphism have not been found in these rocks.

Garnet occurs erratically in the felsic to mafic rocks, as poikiloblasts surrounding pyroxene and as rims around pyroxene and hornblende; it most probably represents a younger stage of metamorphism. Rims and outgrowths of fine biotite and green hornblende are fairly common in mafic bands.

Intermediate to acid rocks may be virtually anhydrous. The basic rocks commonly contain hornblende ± biotite together with pyroxene, but symplectic rims of pyroxene and plagioclase around hornblende may point to a progressive elimination of hornblende. Scapolite is a rare constituent of the more mafic rocks, where it replaced part of the plagioclase as veinlets or large, spongy poikiloblasts. On account of its birefringence, the scapolite would consist of a CO_2-rich variety (meionite).

In the pelitic gneiss, the coarse peak-metamorphic minerals are sillimanite, Mg-rich cordierite, orthopyroxene, biotite, antiperthite, perthite or mesoperthite, and quartz, with opaque minerals, green spinel and rarely corundum. Cordierite shows partial recrystallization to aggregates of fine-grained orthopyroxene, sillimanite, kyanite, andalusite and biotite, and the very rare beryllium mineral, surinamite (de Roever *et al*., 1976). Garnet poikiloblasts occur in some rocks, partly enclosing the fine-grained recrystallization products.

Associated magmatism

Metadolerite dykes are quite common among the banded rocks of the charnockite suite in the core of the Bakhuis belt (de Roever, 1973, 1975). They consist of fine-grained, foliated pyroxene amphibolite and are usually straight and discordant, cutting the banding, but in some cases are partly deformed, showing a synkinematic character (Fig. 3). The dykes are widespread throughout the core of the Bakhuis Mountains. Because such dykes have not been found in the Coeroeni gneiss of southwestern Suriname, their widespread presence and their formation during the granulite-facies metamorphism can be regarded as a special characteristic of the Bakhuis belt metamorphism.

A fairly large anorthosite body (approx. 3×4 km), partly massive and partly layered, has been found in the core of the Bakhuis Mountains (Krook and de Roever, 1975). The layering occurs in the form of centimetre-thick pyroxene bands and thicker leucogabbronoritic bands, with parallel pyroxene orientation. The layering is subvertical, and, based on limited field and drill-core data, subparallel to the banding of the surrounding rocks of the charnockite suite. Two discordant bands of fine-grained pyroxene amphibolite, most probably metadolerite dykes, were found in drill cores. Other anorthosite bodies may have been overlooked because, for example, of preferential weathering.

The southwestern part of the belt shows a rather abrupt transition from the core to large areas composed mainly of dark orthopyroxene granite to tonalite, with abundant gabbroic-ultramafic bodies and only scattered, small lenses of pelitic gneiss and of banded rocks of the charnockite suite (Fig. 2). The abundant presence of orthopyroxene in the pyroxene granite justifies terming these rocks charnockite. They show magmatic as well as metamorphic textures, have a homogeneous, massive appearance, and typically contain antiperthitic plagioclase besides two pyroxenes; they may be similar to the rocks described as Kanuku granulite (Berrange, 1977; see *Geological setting*).

A large pyroxene granite intrusion in the northeast of the Bakhuis belt has a concordant contact with the surrounding pelitic gneiss, whose foliation bends around the intrusion. The greyish granite shows K-feldspar megacrysts and contains clinopyroxene, hornblende and biotite, and, in a few samples, also orthopyroxene. Some samples do not contain any pyroxene, and then hardly differ from the biotite granite outside of the Bakhuis belt. The pyroxene granite resembles the biotite granite geochemically, but differs markedly from the orthopyroxene granite to tonalite.

Small gabbroic and ultramafic bodies (of the so-called De Goeje type; Bosma *et al.*, 1983) occur mainly in the southwestern part of the Bakhuis belt, outside the core of banded rocks of the charnockite suite, although a few bodies do occur within the core of the belt. They are a few kilometres in size and show magmatic differentiation with, for example, a transition from gabbronorite at the top to pyroxenite at the bottom, or a transition from pyroxenite at the top to peridotite.

Dome structure of the Bakhuis belt

At regional scale, the banding is steeply dipping and generally parallel to the belt, but it bends around on its northeastern side. Long lenses of pelitic gneiss also lie parallel to the belt and bend around its northeastern side (Fig. 2). Other rock types appear outside the banded charnockite core of the horst. To the northeast, areas of banded clinopyroxene amphibolite and gneiss are found, metamorphosed in the upper amphibolite facies. To the southwest, a rather abrupt transition, in part coinciding with a N-S fault, occurs between the core and vast areas of dark orthopyroxene granite to tonalite with abundant gabbroic-ultramafic bodies and scattered lenses of pelitic gneiss and of banded rocks of the charnockite suite.

The orientation of the banding and pelitic lenses, and the occurrence of lower-grade metamorphic rocks and orthopyroxene granite in the northeast and southwest respectively provide strong evidence for a dome structure of the Bakhuis Mountains, with an oval, elongate core of banded rocks of the charnockite suite (de Roever, 1973; Dahlberg, 1973). The long sides of the oval core would coincide roughly with the horst faults, although some truncation by the southern fault is evident in the northeast. The faults may have originated during doming of the oval core.

UHT metamorphism in the Bakhuis mountains

Harley (1998) defined UHT metamorphism as a division of medium-pressure granulite-facies metamorphism with P-T conditions of 900 - 1100 °C and 7-13 kbar. The key indicators of UHT conditions are mineral assemblages involving combinations of sapphirine, garnet, aluminous orthopyroxene, cordierite, sillimanite, spinel and quartz in pelite and quartzite. Most of Harley's (op. cit.) key UHT indicators occur locally in pelitic gneiss and quartzite in the Bakhuis Mountains:

- Orthopyroxene + sillimanite + quartz.
- A high level of alumina (up to 10% Al_2O_3) in the orthopyroxene.
- Sapphirine in quartz-rich rocks.

Furthermore, corundum was found in quartz-rich rocks, described so far only from UHT occurrences. Only pyrope-rich garnet is lacking consistently from the peak metamorphic minerals, distinguishing the Bakhuis UHT rocks from many other UHT occurrences.

Most pelitic gneiss of the Bakhuis belt contains Mg-rich cordierite and sillimanite as the common minerals

	Orthopyroxene							Sapphirine			
	Quartzite AB580			Gneiss VG117			Gneiss RG1054	Gneiss VG117	Gneiss VG101	Gneiss WV257	Gneiss RG1054
	Core	Rim	Fine	Core	Rim	Fine	Fine				Sympl.
SiO_2	48.25	50.59	50.73	49.23	49.64	50.81	52.77	13.0	13.9	13.6	12.2
Al_2O_3	10.04	7.20	6.14	8.49	6.08	6.12	4.04	61.3	59.4	58.55	62.2
FeO*	17.86	17.76	16.62	18.42	20.08	17.36	16.16	8.4	10.2	10.3	8.8
MnO	0.87	0.64	0.79	1.11	1.43	1.12	1.53	0.5	0.11	0.08	0.66
MgO	22.64	24.07	24.23	22.91	23.10	24.85	25.70	15.8	16.2	16.5	15.2
CaO	0.05	0.07	0.06	0.04	0.03	-	-	-	-	-	-
Total	99.71	100.33	98.57	100.20	100.36	100.26	100.18	99.0	99.81	99.03	99.06
Si	1.76	1.83	1.87	1.79	1.82	1.84	1.91	1.57	1.68	1.66	1.48
Al	0.43	0.31	0.27	0.37	0.26	0.26	0.17	8.74	8.46	8.42	8.89
Fe^{3+}	0.04	0.03	0.00	0.05	0.10	0.06	0.01	0.12	0.19	0.27	0.15
Fe^{2+}	0.50	0.51	0.51	0.51	0.51	0.46	0.48	0.73	0.84	0.78	0.74
Mn	0.03	0.02	0.02	0.03	0.04	0.03	0.05	0.05	0.01	0.01	0.07
Mg	1.23	1.30	1.33	1.24	1.26	1.34	1.39	2.85	2.92	3.00	2.75
Ca	-	-	-	-	-	-	-	-	-	-	-
Cations	4	4	4	4	4	4	4	14.06	14.11	14.13	14.08
Oxygen	6	6	6	6	6	6	6	20	20	20	20
$Mg/Mg+Fe^{2+}$	0.71	0.73	0.72	0.71	0.71	0.74	0.74	0.80	0.78	0.79	0.79
$Fe^{3+}/Fe\ tot.$	0.07	0.06	0.00	0.09	0.16	0.12	0.02	0.14	0.18	0.25	0.17

Table 1.- Composition of orthopyroxene and sapphirine from the northeastern UHT occurrence (VG 117, VG 101, WV 257, AB 580) and from a possible UHT remnant in the southwest (RG 1054; lower SW asterisk in Fig. 2). Both core and rim were analysed in coarse orthopyroxene crystals. Secondary orthopyroxene occurs as fine intergrowths with sillimanite around coarse orthopyroxene crystals (northeastern occurrence) or in cordierite (RG 1054 from the southwestern remnant). Sapphirine in RG 1054 forms symplectic intergrowths with cordierite. FeO* in the table denotes total iron as FeO.

Tabl. 1.- Composition d'orthopyroxène et de sapphirine provenant de la zone UHT nord-est (VG 117, VG 101, WV 257, AB 580) et de la relique UHT possible du sud-ouest (RG 1054; astérisque plus bas, au sud-ouest, Fig. 2). Les analyses ont été effectuées à la fois au coeur et en périphérie de gros cristaux d'orthopyroxène. De l'orthopyroxène secondaire constitue des intercroissances de fine taille avec la sillimanite autour des gros cristaux d'orthopyroxène (occurrence nord-est) ou dans la cordiérite (RG 1054 pour la relique du sud-ouest). Dans l'échantillon RG 1054 la sapphirine forme des symplectites constituées par l'intercroissance avec la cordiérite. FeO dans la table indique FeO comme Fer total.*

produced during peak metamorphism, which are not indicative of UHT conditions. Characteristic UHT assemblages occur in pelitic rocks in an area on the northeastern side of the Bakhuis belt, and possible remnants have been found at two locations on the southwestern side (Fig. 2).

Methodology

Electron microprobe analysis of sapphirine, cordierite and garnet was carried out with the Cambridge Mark 9 of the Institute of Earth Sciences, Free University, Amsterdam. Analysis of orthopyroxene, sillimanite, biotite and corundum was carried out with the Cameca SX50 electron microprobe of the BRGM.

UHT occurrence on the northeastern side of the belt

Typical UHT rocks occur in an area of 50 km² within a long NW-SE band of pelitic gneiss on the northeastern side of the belt (see Fig. 2). Two rock types have been found, migmatitic gneiss and quartzite. They show banding and foliation in hand specimen and in the field. Good outcrops of the gneiss are scarce in the jungle, being limited to streams in valleys between laterite-capped hills. The quartzite was found only as loose boulders on laterite-strewn slopes.

Gneiss. The gneiss shows narrow dark bands of coarse, oriented orthopyroxene and sillimanite - plus biotite in some rocks - between leucosomes of quartz-antiperthite-perthite or quartz-mesoperthite. Orthopyroxene and sillimanite are intergrown, with sillimanite prisms sticking into poikiloblastic orthopyroxene crystals, or sillimanite interlayered with orthopyroxene. The structure and intergrowth is suggestive of formation from a pre-existing assemblage. Analysed orthopyroxene showed levels of 7½-8½% Al_2O_3 in most of the crystal, with lower levels of 6-4% at the rim (Table 1; see also Appendix, note 2). The sillimanite crystals were not pure Al_2SiO_5, but contained 1-1½% Fe_2O_3 (Table 2). Opaque minerals (magnetite and Fe-Ti oxide) and intergrown green spinel occur between orthopyroxene and sillimanite, and aggregates of magnetite + ilmenite + green spinel occur as inclusions in sillimanite. Preliminary microprobe analyses of green spinel point to zincian (8-10% ZnO) spinel with slightly more Mg than Fe.

Three out of a dozen gneiss samples contained sapphirine as the only dark mineral in their leucosome, or sapphirine and coarse biotite (TiO_2-rich; see Table 2). Sapphirine forms poikiloblasts, ½-1 mm in size, or small, egg-shaped grains in plagioclase – in one case with a quartz rim around the sapphirine grain (Fig. 4). Rarely was sapphirine found in the melanosomes, and then only as inclusions in coarse sillimanite. The sapphirine is

	Cordierite		Biotite		Garnet	Sillimanite			Corundum
	Gneiss RG1054	Gneiss SA776	GneissV G117	Gneiss RG1054	GneissV G117	Quartzite AB580		GneissV G117	Gneiss RG1054
	Sympl.	Coarse	Coarse	Coarse	Coarse	Coarse	Fine	Coarse	Coarse
SiO_2	48.4	49.45	38.28	38.51	39.3	36.63	36.46	37.10	-
Al_2O_3	33.1	33.8	14.94	15.91	22.1	62.06	61.78	61.62	100.29
FeO*	2.2	2.55	9.96	8.73	23.7	1.28	1.25	1.50	0.76
MnO	0.22	0.1	0.09	0.15	4.6	-	-	-	-
MgO	11.6	11.4	16.78	16.93	9.5	-	-	-	-
CaO	-	-	-	0.07	1.4	-	-	-	-
Na_2O	0.09	-	-	0.12	-	-	-	-	-
TiO_2	-	-	3.86	3.64	-	-	-	-	-
K_2O	-	-	9.64	9.94	-	-	-	-	-
Total	95.61	97.3	94.00	93.54	100.6	99.97	99.49	100.2	101.05
Si	4.99	5.00	5.68	5.83	3.00	0.99	0.99	1.00	-
Al	4.02	4.03	2.61	2.84	1.99	1.98	1.98	1.96	1.99
Ti	-	-	0.43	0.42	-	-	-	-	-
Fe^{3+}	-	-	-	-	-	0.03	0.03	0.03	0.01
Fe^{2+}	0.19	0.22	1.24	1.11	1.51	-	-	-	-
Mn	0.02	0.01	0.01	0.02	0.30	-	-	-	-
Mg	1.77	1.72	3.71	3.82	1.08	-	-	-	-
Ca	-	-	-	0.01	0.12	-	-	-	-
Na	0.02	-	-	0.04	-	-	-	-	-
K	-	-	1.82	1.92	-	-	-	-	-
Cations	11.01	10.98	15.50	15.52	8	3	3	3	2
Oxygen	18	18	22	22	12	5	5	5	3
$Mg/Mg+Fe^{2+}$	0.90	0.89	0.75	0.78	0.42	-	-	-	-

Table 2.- Composition of cordierite, biotite, garnet, sillimanite and corundum from the northeastern UHT occurrence (VG 117, AB 580) and from a possible UHT remnant in the southwest (RG 1054 lower, SW asterisk in Fig. 2). Cordierite in RG 1054 forms symplectic intergrowths with sapphirine. The composition of cordierite from a cordierite-sillimanite gneiss (SA 776) outside the northeastern UHT area is given for comparison. Coarse biotite probably formed during granulite-facies metamorphism. Garnet, in poikiloblasts, is most probably secondary. Garnet composition: 50% Alm, 36% Pyr, 10% Sp, 4% Gross. FeO* in the table denotes total iron as FeO.

Tabl. 2.- Composition de cordiérite, biotite, grenat, sillimanite et corindon concernant la zone UHT nord-est (VG 117, AB 580) et la possible relique UHT au sud-ouest (RG 1054; astérisque plus bas au sud-ouest de la Fig. 2). La cordiérite dans RG 1054 forme des textures symplectiques avec la sapphirine. La composition de cordiérite dans un gneiss à cordiérite-sillimanite (SA 776) en dehors de la zone UHT nord-est est donné pour comparaison. Les gros cristaux de biotite se sont formés probablement durant le métamorphisme granulitique. Le grenat, de nature poikiloblastique est probablement secondaire. La composition du grenat est : 50 % Alm, 36 % Pyr, 10 % Sp, 4 % Gross. Dans la table FeO se réfère au FeO total considéré comme FeO.*

peraluminous, near the 7:9:3 composition (Table 1; see also Appendix, note 3), blue pleochroic and Fe^{3+}-bearing. Although only rarely found in contact with quartz, the sapphirine occurs in the quartz-rich leucosome, and certainly was in equilibrium with quartz during its formation.

Quartzite. The quartzite contains centimetre-size, oriented orthopyroxene and sillimanite crystals (Fig. 4). The orthopyroxene crystals contain 9½-10% Al_2O_3 in most of the crystal, with lower Al levels (down to 7%) along the rim (Table 1). The sillimanite contains up to 1.3% Fe_2O_3. Both orthopyroxene and sillimanite are surrounded by symplectic rims of fine to very fine sillimanite and orthopyroxene, with Al_2O_3 levels of 5 - 7½%. Aggregates of opaque minerals, magnetite and Fe-Ti oxides occur between (coarse) orthopyroxene and sillimanite. Green spinel occurs in aggregates of opaque minerals, between sillimanite crystals and as inclusions in sillimanite. Other rocks from the area consist of sillimanite rocks (sillimanitite) with some orthopyroxene and green spinel, or are atypical, such as pure sillimanitite and sillimanite gneiss.

Possible remnants of UHT assemblages on the southwestern side of the belt

Rocks with symplectic cordierite-sapphirine intergrowths were found at the southwestern side of the horst, a) in a pelitic gneiss occurrence amidst orthopyroxene granite and ultramafic-gabbroic rocks outside the banded charnockitic core, and b) in a small pelitic zone just within the core, near its southwest border (Fig. 2). A rock with coarse symplectite from the former occurrence is described here. The cordierite-sapphirine intergrowths occur mainly around or at the end of coarse sillimanite crystals (Fig. 4). The cordierite is Mg-rich and its analyses show a low total, 95-97% (Table 2), suggestive of a high fluid content. The sapphirine is blue pleochroic and Fe^{3+}-bearing, and is peraluminous, being even slightly more Al-rich than the 7:9:3 composition (Table 1). The rock itself is, unfortunately, markedly mylonitic. It consists of dark layers rich in coarse sillimanite, intermediate-size cordierite and biotite (TiO_2-rich; Table 2) and fine or very fine biotite, sillimanite, kyanite and orthopyroxene, and light layers of quartz, feldspar and some cordierite. Locally, the dark layers contain coarse corundum crystals, partly associated with opaque minerals, but also nearly free of them. Fine green spinel occurs between coarse sillimanite and as inclusions in the sillimanite.

The typical UHT association of orthopyroxene + sillimanite + quartz was not found in this rock. The sapphirine-cordierite intergrowths clearly do not represent the peak metamorphic assemblage. Their consistent association with coarse sillimanite crystals may imply that they formed by replacement of a peak mineral(s), probably orthopyroxene, in contact with the coarse sillimanite. Similar cordierite-sapphirine intergrowths after orthopyroxene + sillimanite have been described by Harley and Sheraton (1990), Lal (1997) and Raith *et al.* (1997), among others. The gneiss is quartz-rich, but since the intergrowths formed during localized recrystallization after the peak metamorphism, sapphirine probably did not form in coexistence with quartz.
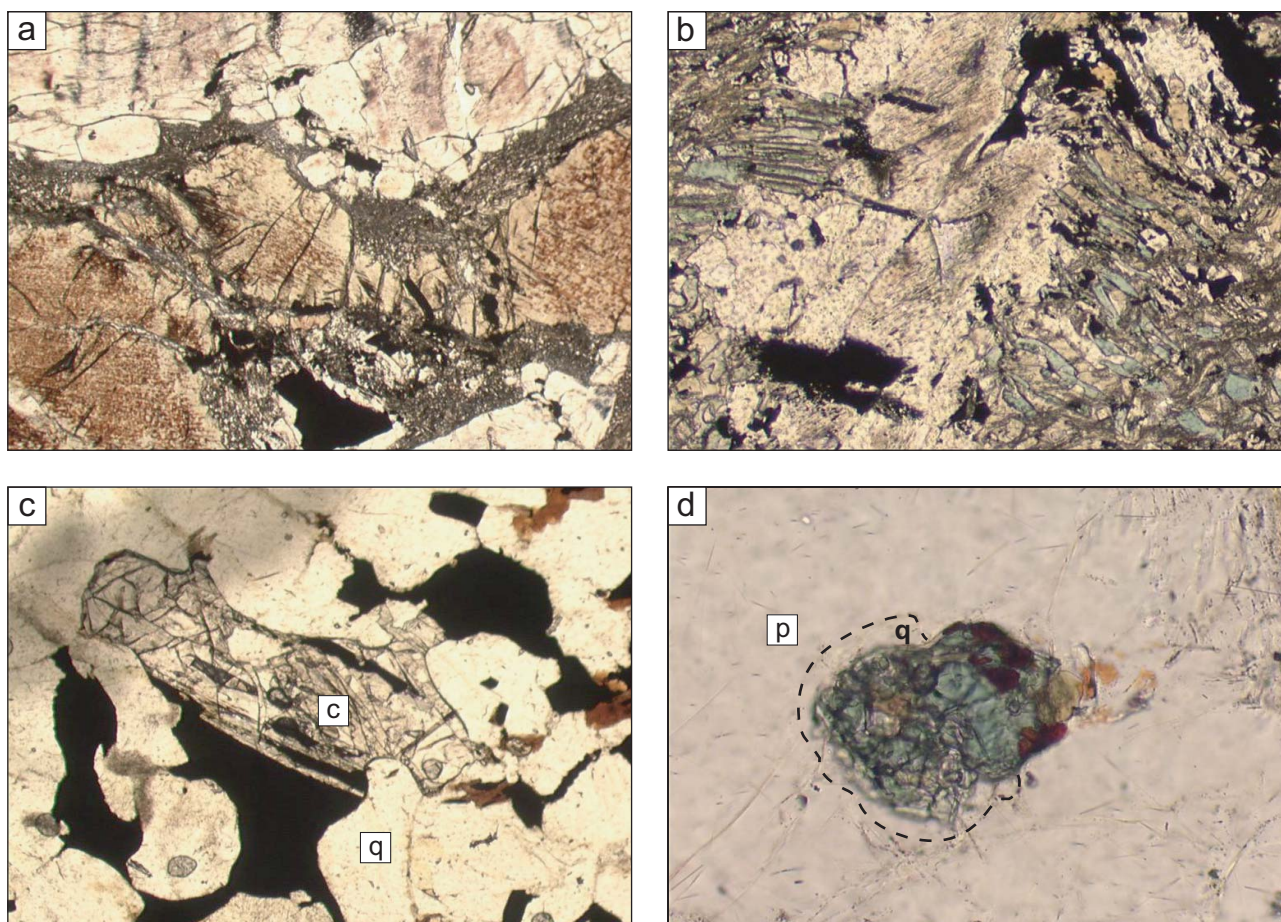
Fig. 4.- Thin-section photographs: a) coarse orthopyroxene and sillimanite (centre/bottom resp. top) with opaque oxides (AB580), b) symplectic sapphirine + cordierite intergrowths around coarse sillimanite in centre (RG1054), c) aggregate of coarse, intergrown magnetite and corundum in contact with quartz (LA 156), d) sapphirine (*ca*. 0.1 mm) with small rim of quartz in plagioclase (VG117). Letters in photographs: c - corundum, q - quartz, p - plagioclase.

Fig. 4.- Photographies de lames minces : a) gros cristaux d'orthopyroxène et de sillimanite coexistant avec des minéraux opaques (AB580), b) texture symplectique avec intercroissance de sapphirine et de cordiérite autour d'un gros grain de sillimanite au centre (RG1054), c) intercroissance de magnétite et de corindon en contact avec du quartz (LA 156), d) sapphirine (ca. 0.1 mm) avec fine couronne de quartz dans du plagioclase (VG117). Les lettres dans les photographies : c - corindon, q - quartz, p - plagioclase.

The other gneiss, from the small pelitic zone just within the core of the belt, not only showed sapphirine in sapphirine-cordierite intergrowths, but also rare inclusions of sapphirine in coarse sillimanite. This suggests that sapphirine in this quartz-rich rock was stable before being surrounded and replaced by coarse sillimanite. Such a double, prograde and retrograde occurrence, has been described elsewhere (e.g. Baba, 2003).

Peak metamorphic conditions of the UHT occurrence

The northeastern occurrence shows two characteristic UHT assemblages:

- orthopyroxene + sillimanite + quartz ± feldspar + opaque minerals + spinel; and

- orthopyroxene + sillimanite + sapphirine + quartz + feldspar + opaque minerals + spinel.

Mg-rich cordierite is one of the main peak-metamorphic minerals in the pelitic gneiss elsewhere in the Bakhuis belt, together with sillimanite. In the UHT occurrence, cordierite is characteristically absent from the gneiss and quartzite, which contain orthopyroxene and sillimanite instead (in the dark layers) or sapphirine (in the leucosome). Its absence is, therefore, considered to be due to the exceptional, ultrahigh-temperature conditions of formation, outside the stability field of cordierite.

The presence of sapphirine in these quartz-rich rocks, locally even in contact with quartz, would point to a formation temperature of at least 1040 °C (Fig. 5). However, this is the minimum temperature of formation of sapphirine + quartz in *reduced rocks*, without significant ferric iron. The consistent presence of magnetite in the gneiss and quartzite points to a high fO_2. At high fO_2, with substantial Fe^{3+} replacing Al, sapphirine + quartz may form below 1040 °C, as described for the northern part of the
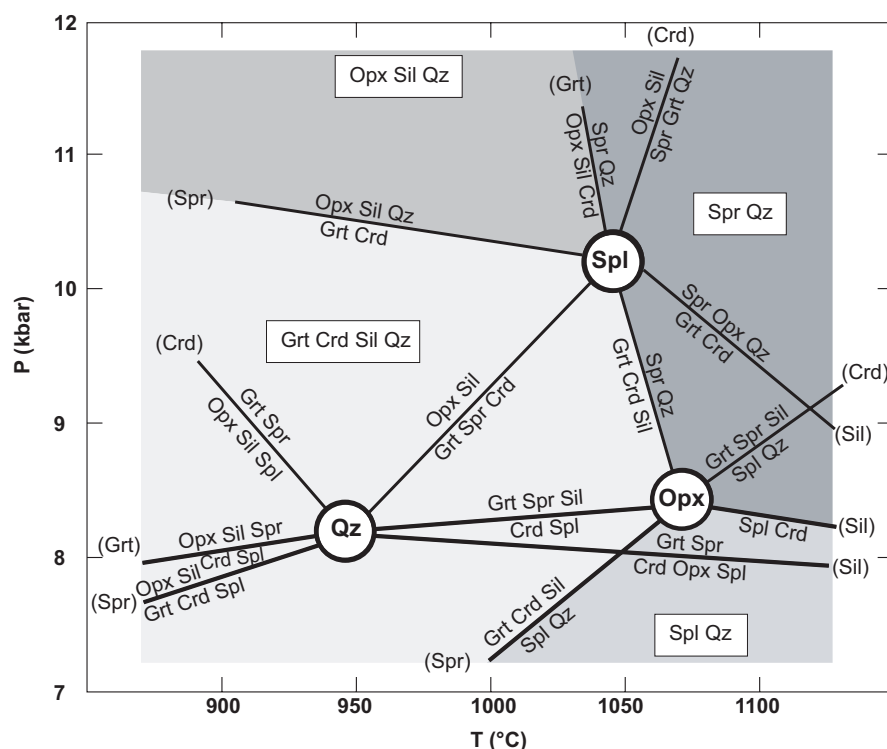
Fig. 5.- P-T diagram of the model FMAS system grid for low fO_2 pelite (after Harley, 1998). Fields of key FMAS assemblages (Spr + Qz, Opx + Sil + Qz, Spl + Qz and Grt + Crd + Sil + Qz) are distinguished by shading. Note the position of the invariant point [Spl]. Abbreviations: Spr - sapphirine, Opx - orthopyroxene, Sil - sillimanite, Spl - spinel, Grt - garnet, Crd - cordierite, Qz - quartz.

Fig. 5.- Diagramme P-T utilisant la grille pétrogénétique du système FMAS s'appliquant à des pélites pour des conditions de faible fugacité d'oxygène (d'après Harley, 1998). Les champs des assemblages clés dans le système FMAS (Spr + Qz, Opx + Sil + Qz, Spl + Qz et Grt + Crd + Sil + Qz) sont distingués en figurés grisés. Notez la position du point invariant [Spl]. Abbréviations: Spr - sapphirine, Opx - orthopyroxène, Sil - sillimanite, Spl - spinelle, Grt - grenat, Crd - cordierite, Qz - quartz.

900 °C. Experiments by Das *et al.* (2003) point to at least 8 kb. Dasgupta *et al.* (1995), using the Al_2O_3 isopleths provided in the semi-empirical grid of Hensen and Harley (1990), estimated the formation temperature of orthopyroxene with 8-8½% Al_2O_3 to be at least 950 °C, despite formation at high fO_2. However, it is assumed here that high fO_2 would cause at least some reduction of the formation temperature of aluminous ortho-pyroxene, compared to that at low fO_2 – otherwise the 10% Al_2O_3 in orthopyroxene from the quartzite would point to an unrealistic high T of > 1050 °C. Similar aluminous orthopyroxene (7 - 10% Al_2O_3) in oxidized rocks at Sunkarametta (Eastern Ghats, India) was estimated to have formed at approx. 950 °C (Bose *et al.*, 2000).

Many UHT occurrences show garnet as a widely distributed phase. However, sapphirine-bearing rocks from Wilson Lake, (northern) Eastern Ghats, Labwor Hills and In Ouzzal (Algeria) almost invariably lack garnet, but contain spinel in addition to sapphirine, cordierite and orthopyroxene, and show associated opaque minerals, including magnetite, hemoilmenite and hematite, indicative of higher fO_2 (Harley, 1998). Higher oxygen fugacities would lead to a restricted occurrence, or even absence, of garnet and to its replacement by spinel (Hensen, 1986; Powell and Sandiford, 1988). Most probably a higher oxygen fugacity explains the consistent absence of garnet from the peak metamorphic assemblages in the pelitic gneiss and quartzite of the Bakhuis UHT occurrence. These rocks contain magnetite, Fe-Ti oxide and spinel, and show appreciable Fe^{3+} in sapphirine and sillimanite, all consistent with a higher oxygen fugacity. The role of spinel is far from clear, because it occurs only in small amounts, commonly in aggregates with magnetite and Fe-Ti oxide (with more opaque material than spinel), between sillimanite and as inclusions in sillimanite. Aggregates of magnetite, Fe-Ti oxide and green spinel may have formed by exsolution from a Fe-rich spinel solid solution.

Eastern Ghats, India (Dasgupta *et al.*, 1995), Labwor Hills, Uganda (Sandiford *et al.*, 1987), and Wilson Lake, Canada (Arima *et al.*, 1986). The temperatures deduced for these occurrences are 950 - 1050 °C, still in the UHT range (Harley, 1998). An experimental study by Das *et al.* (2003) showed that a minimum of 950 °C is required for the formation of sapphirine + quartz at high fO_2 in such rocks.

The orthopyroxene + sillimanite + quartz assemblage would point to pressures in excess of 8 kb and temperatures greater than 900 °C at low fO_2 in the KFMASH system (e.g. Harley, 1998). The presence of 8½% Al_2O_3 in the orthopyroxene from the gneiss would point to T > 950 °C for the reduced system, whereas the 10% Al_2O_3 in the orthopyroxene from the quartzite would point to T > 1050 °C. The orthopyroxene itself contains insignificant Fe^{3+}, but associated Fe oxide and Fe^{3+} in the accompanying sillimanite points to a high fO_2, which probably implies a lower temperature of formation. The pressure and temperature required to produce orthopyroxene + sillimanite + quartz at high fO_2 were estimated by Dasgupta *et al.* (1995), based partly on experimental data from Carrington and Harley (1995), to be at least 8½kb and

Metamorphism of the surrounding rocks

Except for the northeastern occurrence, pelitic gneiss in the Bakhuis horst does not show typical UHT assemblages with, for example, sapphirine + quartz. It commonly shows

cordierite-sillimanite assemblages (without coeval garnet). Its close spatial association with UHT assemblages in the northeast of the Bakhuis belt suggests that P-T conditions during its metamorphism were not much different from the UHT P-T conditions, but just insufficient to produce sapphirine + quartz and common orthopyroxene + sillimanite.

Green spinel and opaque minerals, including magnetite and Fe-Ti oxides, are common accessories in the pelitic gneiss. The green spinel from two locations was found to be rich in Zn $(Mg_{0.2-0.4}Fe_{0.4}Zn_{0.4-0.2})Al_2O_4$. The presence of spinel and Fe oxides and absence of coeval garnet suggest a high oxygen fugacity during metamorphism, similar to the UHT metamorphism. Opaque minerals and green spinel commonly occur together in the gneiss, either in aggregates with more opaque material or in aggregates with similar amounts of spinel and magnetite. The latter occurrence is suggestive of granule exsolution from a magnetite-spinel solid solution (Waters, 1991; Dasgupta *et al*., 1995) that was stable at T > 860 °C (Turnock and Eugster, 1962) or even > 900 °C (Nell and Wood, 1989).

Cordierite is typically Mg-rich (X_{Mg} ca. 0.9; see Table 2), which would point to 9-10 kb if it were associated with garnet. For cordierite-spinel-quartz assemblages, high Mg in the cordierite would require a somewhat lower, but still high, P (Waters, 1991). The cordierite analyses show a low total (97-98%) which may point to a high fluid content.

In a small part of the pelitic gneiss samples, but occurring throughout the belt, cordierite + sillimanite are accompanied by coarse orthopyroxene. This assemblage may represent a transition to UHT assemblages, by containing orthopyroxene + sillimanite + quartz + cordierite. More study of the pelitic gneiss is needed, in particular of that with orthopyroxene, but the available evidence suggests near-UHT conditions during peak metamorphism of the pelitic gneiss in the Bakhuis belt outside the UHT occurrence.

As regards the associated banded rocks of the charnockite suite, no evidence for UHT metamorphism has yet been found. UHT assemblages are typically found in pelitic gneiss and quartzite, whereas quartzofeldspathic and basic lithologies may largely or completely lack evidence of UHT metamorphism (Harley, 1998). It is quite common to find a lower T indicated by the pyroxene geothermometry of these rocks because of widespread and prolonged re-equilibration during retrograde metamorphism (Harley, 1998). Preliminary results of pyroxene geothermometry and amphibole-plagioclase geothermometry in mafic Bakhuis rocks point to temperatures of only 750 – 800 °C (Odon and Enjolvy, 2003).

The banded rocks of the charnockite suite consistently lack peak metamorphic garnet. Magnetite and Fe-Ti oxides have been found in analysed samples; moreover, magnetite

can be assumed to be widespread and common in the banded rocks of the charnockite suite, because of the strong and characteristic magnetic signature of the Bakhuis high-grade rocks on aeromagnetic maps. The lack of garnet in the peak metamorphic assemblage in the banded charnockitic rocks could be interpreted as pointing to typical lower-pressure granulite-facies conditions. However, the local association with UHT pelitic gneiss in the northeast indicates that at least the nearby banded rocks of the charnockite suite underwent UHT metamorphism, but without production of indicative minerals such as garnet, due in particular to higher oxygen fugacity.

Corundum in quartz-rich gneiss: evidence of UHT metamorphism?

The gneiss with coarse cordierite-sapphirine from the southwest contains corundum in thin mafic layers between quartz-rich layers. The mafic layers consist of fine, intermediate and coarse minerals, formed at different times. The corundum is quite coarse and is generally associated with opaque minerals. In some cases the corundum crystals are coarser than the aggregates of opaque material. Corundum crystals have also been found locally with hardly any accompanying opaque minerals. No direct contacts of corundum with quartz were seen, but widespread recrystallization and mylonitization in this rock obscured most of the original grain contacts. Contacts of corundum with sillimanite and cordierite were observed.

Pure corundum cannot be formed stably in quartz-bearing rocks under any crustal conditions, and corundum + quartz is metastable with respect to sillimanite at those conditions (Harlov and Newton, 1993; Harlov and Milke, 2002). However, corundum in contact with quartz has been described many times from UHT rocks (and in a few cases also from restitic contact-metamorphosed rocks; see Harlov and Milke, 2002). In most cases corundum occurs in magnetite, having formed either as an exsolution product from a Fe-rich spinel solid solution with excess Al_2O_3, or as an oxidation product from hercynitic spinel (Ellis *et al*., 1980; Perchuk *et al*., 1989; Dasgupta and Ehl, 1993). At the In Ouzzal UHT occurrence (Algeria), coarse primary corundum occurs in aggregates with coarse magnetite and is in contact with quartz (Guiraud *et al*., 1996). The corundum probably formed by exsolution from an Fe-rich spinel solid solution during cooling; it is not pure, but has a low Fe_2O_3 content (0.7%). It has been suggested that the corundum possibly formed stably with quartz, because quartz and corundum were in contact, without reaction rims, despite the high temperature involved. It was considered to have formed during the UHT metamorphism, on the assumption that Fe_2O_3 replacement of Al_2O_3 would change its stability field, but such a change could not be demonstrated from available thermodynamic data (Guiraud *et al*., 1996). In the Rayagada UHT occurrence of north-central Eastern Ghats (India),

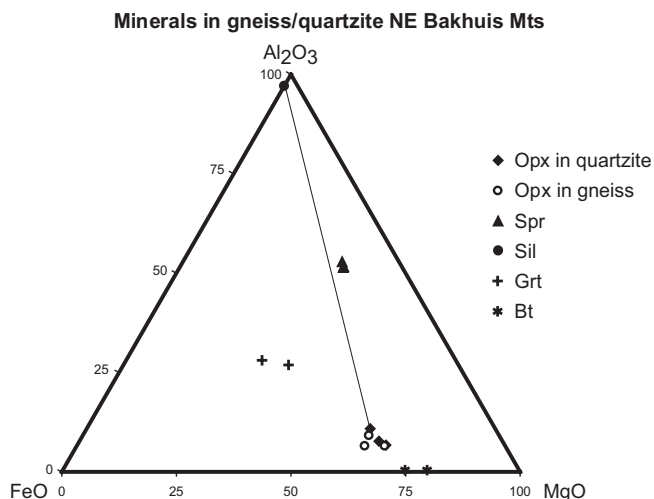**Minerals in gneiss/quartzite NE Bakhuis Mts**

Fig. 6.- AFM compositional plots for primary and secondary minerals in pelitic gneiss and quartzite from the northeastern UHT occurrence. Abbreviations: see Fig. 5. Bt - biotite.

Fig. 6.- Report dans un triangle AFM des minéraux primaires et secondaires de gneiss pélitique et de quartzite se rapportant à la zone UHT nord-est. Abbréviations : voir Fig. 5. Bt - biotite.

millimetre-size porphyroblastic corundum and quartz grains were found separated by sillimanite coronas. Corundum + quartz + garnet + spinel was considered to be the peak UHT metamorphic assemblage (Shaw and Arima, 1998), formed at rather high fO_2. Examples of quartz in contact with corundum formed in magnetite most probably imply different ages of corundum and quartz. This would agree with a metastable contact, as argued by Harlov and Milke (2002). However, the example provided by Shaw and Arima (1998) points to the contemporaneous formation of corundum and quartz during peak UHT metamorphism and deformation. Harlov and Milke (2002) do not present an explanation for the Rayagada occurrence, and this example of porphyroblastic corundum and quartz provides the best possibility so far for the stable formation of corundum + quartz. The corundum is Fe^{3+}-bearing, suggesting that Fe or fO_2 played some role in expanding its stability field to crustal conditions.

The corundum in the Bakhuis gneiss is impure, Fe^{3+}-bearing (Table 2). In most cases it is associated with much opaque material (magnetite and less Fe-Ti oxide) as in the In Ouzzal occurrence. Some coarse corundum crystals are associated with small, or fairly small, amounts of associated opaque material and may not have been formed upon spinel exsolution. The grains are coarse, suggesting that corundum is a peak metamorphic mineral. The Fe^{3+} level of the corundum would agree with the conditions of peak metamorphism: oxygen fugacity was probably rather high, as indicated by Fe^{3+} in the sillimanite and by the presence of green spinel and magnetite. Although the mylonitic and markedly recrystallized rock does not show corundum in contact with quartz, it is possible that part of the coarse,

impure, corundum formed contemporaneously with quartz at UHT or near-UHT conditions. As the corundum-quartz occurrence in India (Shaw and Arima, 1998) and an occurrence in Norway (Krogh, 1977; Fe^{3+}-bearing corundum inclusions in quartz) were formed under UHT or near-UHT conditions, it is possible that (coarse) impure corundum + quartz is typical of oxidized UHT rocks. This would be useful for unravelling the metamorphism in the Bakhuis belt, because corundum is more common than sapphirine in quartz-rich pelitic gneiss.

Another corundum-bearing rock, from the core of the Bakhuis belt, is very similar to the corundum + quartz occurrence at In Ouzzal. It shows aggregates of large corundum crystals grown through coarse magnetite grains, with corundum in contact with quartz (Fig. 4). It is a massive garnet-rich leuco-enderbitic rock with hardly any deformation, but contains no minerals pointing to UHT metamorphism. The rock (part of drill-core LA 156) occurs in the centre of the core of the Bakhuis belt, which consists almost entirely of banded rocks of the charnockite suite, nearly without any pelitic intercalations. This presence of corundum plus quartz is the first indication of exceptional conditions for this central part of the belt.

Discussion of the P-T path in the UHT rocks

Prograde metamorphism

Quartzite and most gneiss samples in the northeastern occurrence contain sillimanite + orthopyroxene + quartz, but some gneiss samples show sapphirine + quartz and sillimanite + orthopyroxene + quartz in different parts of the rock. Sillimanite + orthopyroxene + quartz (+ opaque minerals + spinel) is therefore considered to represent the peak metamorphic assemblage, without sapphirine. When plotted on an AFM diagram, the orthopyroxene − sillimanite tieline nearly passes through the sapphirine plots (Fig. 6). Sapphirine in the leucosome was most probably not in equilibrium with the sillimanite + orthopyroxene + quartz association; it is considered to be a remnant of an older assemblage. Sapphirine was also found - but only rarely - as inclusions in coarse sillimanite in the sillimanite-orthopyroxene bands. This suggests that sapphirine formed and existed as a stable phase before being enclosed/replaced by sillimanite.

Orthopyroxene and sillimanite in the gneiss form intergrowths, as if they replaced a former mineral (or minerals). If this is the case, the former mineral was probably cordierite, because cordierite is very common in gneiss outside the UHT occurrence; a replacement of former pyrope-rich garnet is hardly probable, since this would have to be very Mg-rich, and since coeval garnet was not found in the gneiss. The early assemblage with cordierite might have been largely identical to the cordierite-sillimanite-spinel-quartz assemblage so common in the pelitic gneiss of the Bakhuis belt outside the UHT occurrence.

Thus, petrological evidence suggests an early assemblage (I) with cordierite + sillimanite, followed by an assemblage (II) with sapphirine and quartz, and finally the peak assemblage (III) orthopyroxene + sillimanite + quartz. At least assemblages II and III, and probably also assemblage I, were formed at high oxygen fugacity, with magnetite + Fe-Ti oxide + spinel, and with Fe^{3+} in sapphirine and sillimanite. The concentration of iron as Fe^{2+} in Fe oxide and its partial oxidation to Fe^{3+} in Fe oxide and silicates, resulted in relatively Mg-rich silicate phases, such as the orthopyroxene (see Fig. 6).

In view of the rather small number of silicate phases in the assemblages, petrogenetic grids involving mineral equilibria in the $FeO-MgO-Al_2O_3-SiO_2$ (FMAS) and KFMASH (with additional K_2O and H_2O) systems can be used to analyse the changes in pressure and temperature. A detailed diagram has been constructed for the FMAS system at low fO_2 (Fig. 5). However, there is considerable uncertainty for the system at high oxygen fugacity, at which garnet assemblages (around the [spinel] invariant point in Fig. 5) are replaced by spinel assemblages (around the [garnet] invariant point). Assemblages I-III, with cordierite, orthopyroxene, sapphirine, quartz and spinel, correspond to assemblages around the [garnet] invariant point (Hensen, 1986; Powell and Sandiford, 1988; Hensen and Harley, 1990). Plotting the assemblages around the [garnet] invariant point shows a counterclockwise P-T path for the prograde metamorphism (Fig. 7), going first towards higher temperature, then to lower temperature, with overall some increase in pressure.

The P-T conditions of the [garnet] invariant point in the KFMASH grid are poorly known. Dasgupta *et al* (1995) adapted the KFMASH petrogenetic grid at low fO_2 to a partial grid for high fO_2 to describe oxidized UHT rocks from Eastern Ghats (India). The grid is applicable only to rocks showing melting, but the pelitic rocks from the Bakhuis belt are migmatic and underwent partial melting during the granulite-facies metamorphism. The KFMASH invariant points can be placed within a narrow P-T range of 8-10 kb at 900 - 1000 °C (Dasgupta *et al.*, 1995). The grid situates the [garnet] invariant point near 950 °C (see Fig. 8), implying sapphirine + quartz stability at such a relatively low temperature in oxidized rocks. On the basis of experimental data from Carrington and Harley (1995), Dasgupta *et al.*
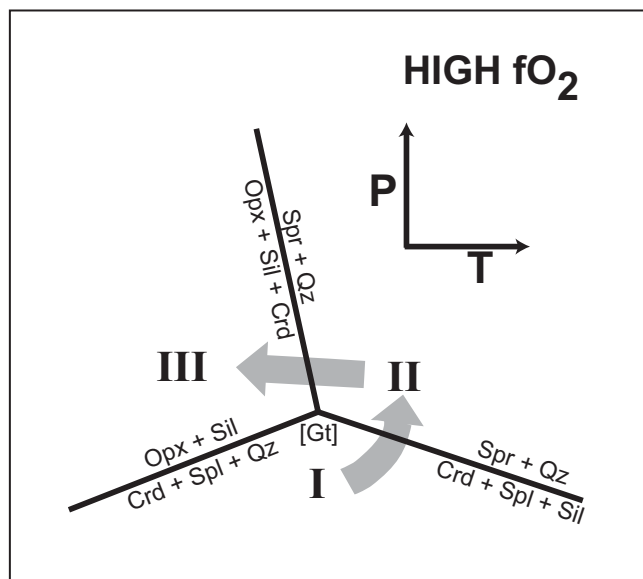

Fig. 7.- Schematic P-T relationships between assemblages I, II and III in the northeastern UHT occurrence, illustrated in the model FMAS system grid at high fO_2, around the [Garnet] invariant point (after Hensen, 1986). Assemblage I - cordierite + sillimanite, Assemblage II - sapphirine + quartz, Assemblage III - orthopyroxene + sillimanite + quartz. Univariant reactions are also shown. Abbreviations: see Fig. 5.

Fig. 7.- Relations P-T schématiques entre les assemblages I, II et III se rapportant à la zone UHT nord-est, et illustrées dans la grille pétrogénétique du système FMAS pour des conditions de forte fugacité d'oxygène, autour du point invariant grenat [Garnet] (d'après Hensen, 1986). Assemblage I - cordiérite + sillimanite, Assemblage II - sapphirine + quartz, Assemblage III - orthopyroxène + sillimanite + quartz. Les réactions univariantes sont également figurées. Abbréviations : voir Fig. 5.
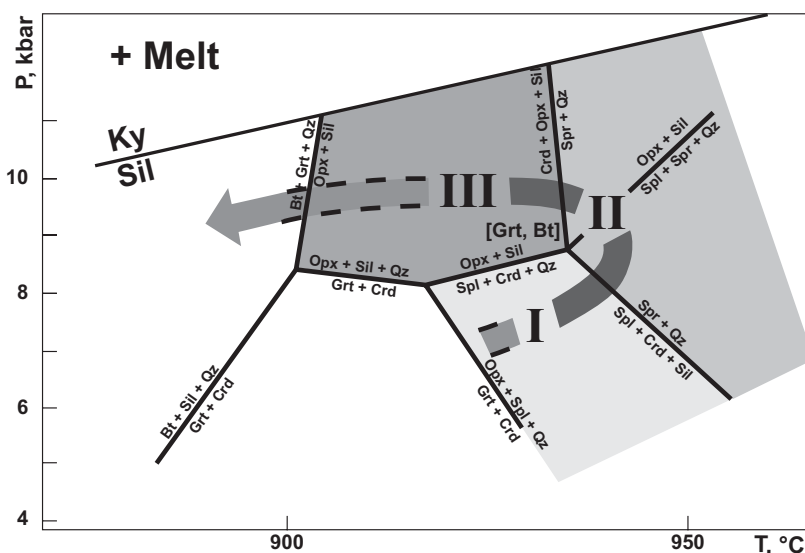
Fig. 8.- The P-T diagram for the KFMASH system grid for pelite at high fO_2 (simplified from Dasgupta *et al.,* 1995), showing the suggested P-T path for the prograde metamorphism (assemblages I → II → III) and the retrograde metamorphism of the gneiss and quartzite in the northeastern UHT occurrence. Univariant reactions and the kyanite/sillimanite transition are also shown. The Spr + Qz and the Sil + Opx + Qz fields are given in two shades of grey. Abbreviations: see Fig. 5; bt – biotite, ky – kyanite.

Fig. 8.- Diagramme PT dans la grille pétrogénétique du système KFMASH s'appliquant à des pélites pour des conditions de forte fugacité d'oxygène (simplifié d'après Dasgupta et al., 1995), montrant le trajet P-T suggéré pour le métamorphisme prograde (assemblages I → II → III) et le métamorphisme rétrograde de gneiss et de quartzite dans la zone UHT nord-est. Les réactions univariantes et la transition disthène/sillimanite sont aussi figurées. Les champs Spr + Qz et Sil + Opx + Qz sont représentés par deux figurés en grisé. Abbréviations : voir Fig. 5 ; bt – biotite, ky – disthène.

(1995) assumed that the orthopyroxene + sillimanite + quartz assemblage would require about 8½kb, and that the [garnet] invariant point would be situated at 8½– 9 kb. The unique orthopyroxene + sillimanite + quartz + spinel assemblage would be stable only within a small P-T window of 8 - 10 kb at 900 -1000 °C (Dasgupta *et al.*, 1995), being also bound by the upper stability of spinel + quartz. The suggested prograde P-T path of the Bakhuis UHT rocks (path I - II - III) is shown in a simplified version of the KFMASH petrogenetic grid of Dasgupta *et al.* (1995) (Fig. 8). Quite recently, Das *et al.* (2003) established an experimentally constrained KFMASH grid that differs from the grid of Dasgupta *et al.* (1995) in the incorporation of osumilite. The experimental study confirmed the small P-T window of 8 - 10 kb at 900 - 1000 °C for the orthopyroxene + sillimanite + quartz + spinel assemblage (Das *et al.*, 2003).

Retrograde metamorphism

The northeastern UHT occurrence. Gneiss and quartzite show clear evidence of retrograde metamorphism. Orthopyroxene crystals in the quartzite show a reduction in the Al_2O_3 level from 9½-10% in the bulk of the crystal down to 6% in the narrow rims, and are surrounded by intergrowths of fine orthopyroxene with similar low Al_2O_3 level and (Fe^{3+}-bearing) sillimanite. Orthopyroxene crystals in the gneiss show the same reduction in Al_2O_3 level at the rim and in fine intergrowths. This reduction in Al_2O_3 level points to a P-T decrease within the granulite-facies (at rather high fO_2). Since the Al isopleths for orthopyroxene in equilibrium with sillimanite (or cordierite), garnet and quartz in the FMAS P,T grid are steep (Hensen and Harley, 1990), the reduction of the Al level is assumed to require an isobaric or near isobaric cooling (IBC) path. Such a path would also be in line with the later formation of kyanite + biotite at the expense of sapphirine, under amphibolite-facies conditions. The appearance of retrograde biotite replacing sapphirine in nearly H_2O-free rocks most probably indicates H_2O introduction associated with a younger deformation stage.

One of the gneiss samples contained garnet poikiloblasts. They do not look like remnants and most probably formed at a late stage. The analysed garnet is almandine-rich, with a substantial pyrope level (Table 2). It probably formed at lower fO_2 than the peak metamorphic assemblage (in pelitic gneiss from surrounding areas, garnet poikiloblasts were found associated with rutile). Garnet-biotite thermometry for a pelitic gneiss from outside the UHT occurrence, with garnet of similar composition, pointed to a temperature in the 620-720 °C range (Odon and Enjolvy, 2003).

The southwestern UHT (?) remnants. Cordierite-sapphirine intergrowths, such as found in the two southwestern occurrences, have commonly been interpreted as evidence for isothermal, or near isothermal, decompression (ITD; Harley and Sheraton, 1990; Lal, 1997; Raith *et al.*, 1997). The initial ITD-like path would fit with the onset of doming, but other explanations could also be put forward.

Parts of the cordierite grains in the gneiss were recrystallized into fine- to very fine orthopyroxene, sillimanite, biotite and kyanite. The four minerals may occur together, but sillimanite is usually associated with orthopyroxene and kyanite usually with biotite. Fine orthopyroxene associated with fine sillimanite, contained 2½-5½% Al_2O_3 (Table 1). Small orthopyroxene rims on (coarse) biotite grains and along biotite cleavage contained about 5½% Al_2O_3. The final recrystallization into kyanite + biotite would be in line with a later IBC- or near-IBC-like path, as for the northeastern UHT occurrence. The intervening stage of cordierite replacement by (low Al) orthopyroxene + sillimanite may also have occurred during a near-IBC-like path. However, it may have been more complex. The retrograde metamorphism in the Bakhuis belt requires further study, the more so since partial replacement of cordierite occurs at regional scale, throughout the Bakhuis belt (de Roever, 1973; de Roever *et al.*, 1976; see also Kroonenberg, 1976).

Comparison with other granulite occurrences in the Guiana Shield

So far, no typical UHT assemblages have been reported from the other granulite-facies domains in the Guiana Shield, i.e. at Imataca, Amapá and Kanuku-Coeroeni.

Granulite-facies rocks in the Imataca belt comprise pelitic rocks with widespread cordierite, garnet, sillimanite, biotite, orthopyroxene and Fe-Ti oxides (Dougan, 1974). P-T conditions for the metamorphism were estimated on the basis of two-pyroxene geothermometry and garnet-orthopyroxene assemblages to be 8-8½kb and 750-800 °C. A maximum level of 6% Al_2O_3 was found for orthopyroxene from a garnet-bearing metanorite (Swapp and Onstott, 1989).

In central Amapá two-pyroxene granulite is typical, and the pelitic rocks show garnet-bearing assemblages (Avelar, 2002).

In the Kanuku complex in Guyana, the main minerals in the pelitic gneiss are cordierite + sillimanite + garnet + biotite, but orthopyroxene + cordierite + sillimanite is fairly common in the Kanuku Mountains (Berrange, 1977). The widespread cordierite, sillimanite and garnet would point to lower-pressure granulite facies conditions, but the orthopyroxene-bearing rocks might represent a possible transition. So far, characteristic UHT assemblages have not been found. The same marked magnetic signature was found for the high-grade rocks in the Kanuku horst as in the

Bakhuis horst, probably due to the widespread occurrence of Fe oxides. For example, local quartzite contains magnetite + hematite, and more rarely magnetite + hematite + green spinel (Berrange, 1977), indicative of high oxygen fugacity.

The Coeroeni gneiss in southwestern Suriname comprise amphibolite-facies and granulite-facies rocks. The granulite-facies zone is defined with the appearance of orthopyroxene in the basic rocks, whereas the pelitic rocks in the zone contain cordierite, garnet and sillimanite. P-T conditions of the granulite-facies metamorphism were estimated to be about 6-8 kb and 800 °C at $pH_2O < P_{total}$ (Kroonenberg, 1976). A detailed study of retrograde metamorphism showed a near-isobaric cooling path (Kroonenberg, op. cit.).

NE UHT occurrence	possible UHT remnants in the SW
Cordierite? + Sillimanite + Spinel	
↓	
Sapphirine + Quartz + Sillimanite + Spinel?	Sapphirine + Quartz + Sillimanite + Spinel?
↓	↓
Orthopyroxene + Sillimanite + Quartz (with 8-10% Al_2O_3 in orthopyroxene) + Spinel + Fe oxides	Orthopyroxene? + **Sillimanite + Quartz**
↓	
	Sapphirine + Cordierite
Orthopyroxene + Sillimanite + Quartz (with 4-7% Al_2O_3 in orthopyroxene)	↓
	Orthopyroxene + Sillimanite + quartz (with 2-5% Al_2O_3 in orthopyroxene)
↓	↓
Biotite + Kyanite	Biotite + Kyanite
↓	↓
Garnet poikiloblasts	(Garnet poikiloblasts) (in surroundings)

Tabl. 3.- Characteristic mineral assemblages formed during prograde and retrograde metamorphism in the northeastern UHT occurrence and the possible remnants of UHT metamorphism in the southwestern part of the belt. The rare presence of early sapphirine (inclusions in sillimanite) and suggested original presence of orthopyroxene in the possible remnants in the southwest suggest a similar counterclockwise prograde P-T path as for the northeastern UHT occurrence.

Table 3.- Assemblages minéralogiques caractéristiques formés durant le métamorphisme prograde et rétrograde dans la zone UHT nord-est et dans les reliques UHT possibles du sud-ouest. La rare présence de sapphirine précoce (en inclusions dans la sillimanite) et la présence suggérée d'orthopyroxène initial dans les reliques possibles UHT du sud-ouest suggèrent un trajet P-T antihoraire comparable à celui du trajet P-T prograde de la zone UHT nord-est.
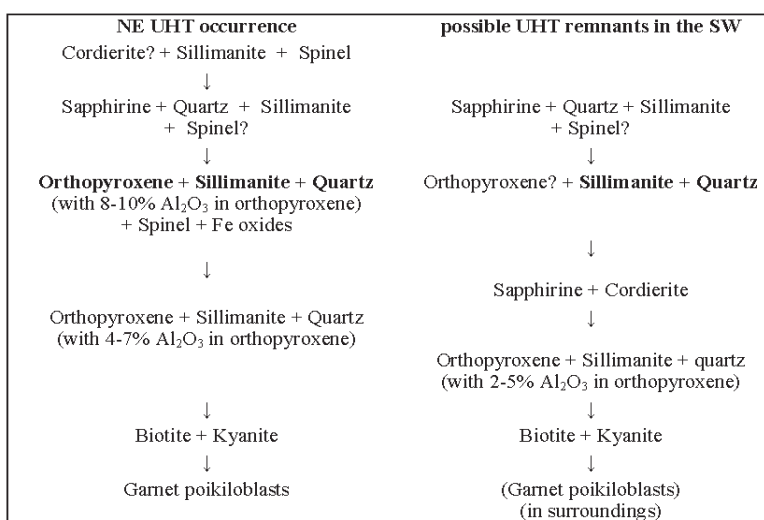
Geochronological results

For a long time it was thought that the high-grade rocks of the Bakhuis belt (Falawatra Group) were polymetamorphic rocks, with possibly an Archean age, as found in Imataca and Amapá. Rb-Sr dating by Priem *et al.* (1978) pointed to an age between 2.0 and 2.4 Ga. Zircon U-Pb dating of one sample has led to the conclusion that the major migmatization and metamorphism occurred around 2026 ± 20 Ma. Nd-Sm whole-rock dating (Ben Othman *et al.*, 1984) of a single sample gave a model age of 2.3 Ga.

In this chapter, we present detailed integrated Sm-Nd investigations on whole rocks and Pb-Pb isotopic studies on zircons from granulites, dykes and cross-cutting veins, in order to decipher the exact time of formation of the granulite parageneses and their protolith.

Sample descriptions

Sample preparation for Sm-Nd dating on whole rocks, and also for zircon and monazite extraction, was done at the BRGM laboratory for mineral-characterization in Orléans, France.

The selected samples for the zircon Pb-evaporation, monazite Pb-microprobe and Sm-Nd whole-rock dating came from different locations in the Bakhuis belt, as shown on Figure 2. They are: two samples of enderbitic gneiss (Su3f and Su12c); a garnet-sillimanite-bearing gneiss (Su11d); two samples of synfolial leucogranite layers (Su10e1 and Su10e2) in garnet-sillimanite gneiss, corresponding to *in situ* melting;

garnet-bearing gneiss (LC57-2a) and a garnet-bearing pegmatite layer (LC57-2b) in the gneiss; two samples of a discordant recrystallized metadolerite dyke within enderbitic gneiss, one from a fine-grained foliated part (Su12aDF) and one from a part with millimetre-size leucocratic veins suggesting incipient melting (Su12aDV); three samples of late pegmatite (Su14a and Su14c from a discordant vein; Su15 from a discordant sheared vein) that crosscuts the NE-SW-trending granulite in the area of the Blanche Marie Falls; a mylonitic orthopyroxene-bearing granite (a true magmatic charnockite; Su6b); and a drill-core of anorthosite (ER117) from the core of the Bakhuis Mountains.

Experimental procedures

Eight of the high-grade rock samples and the anorthosite sample from the Bakhuis Mountains were dated by the Pb-Pb evaporation method on zircon (Kober 1986, 1987) at the geochronological laboratories of BRGM (Orléans, France) and UFPa (Belém, Brazil).

At UFPa, isotope analyses on samples Su12aDF and DV, Su6b, Su15, LC57-2b and ER117 were performed on a Finnigan MAT262 mass spectrometer in dynamic mode, using an ion counting detector. $^{207}Pb/^{206}Pb$ ratios were corrected of a mass discrimination factor of 0.12% ± 0.03 per a.m.u., determined by repeated measurements of NBS-982 Pb standard. Analyses with $^{206}Pb/^{204}Pb$ ratios lower than 2500 were discarded and not shown in the table of isotopic data. Common Pb correction was done using the Stacey and Kramers (1975) model at the age of the grain.
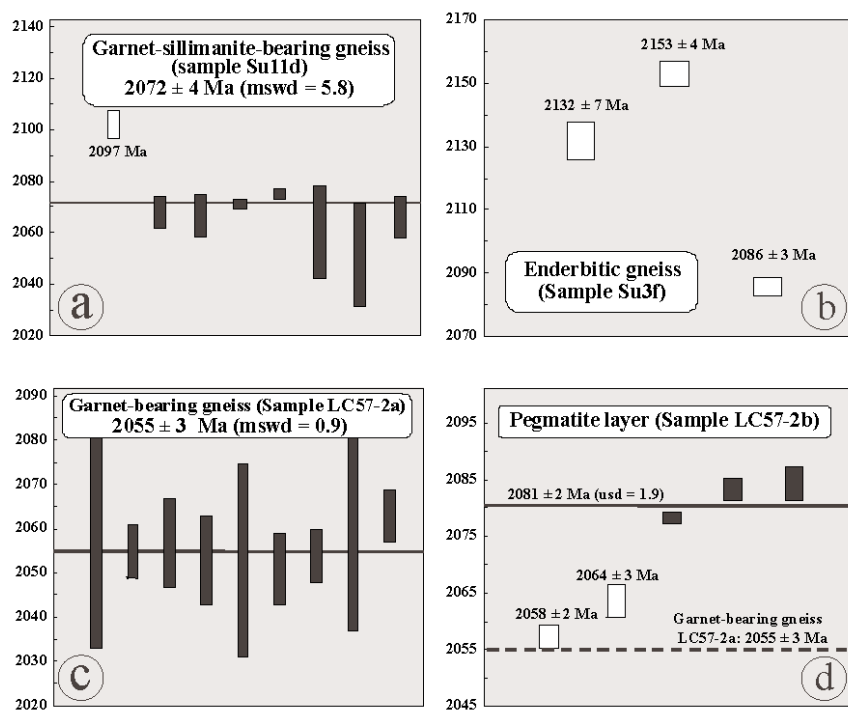
Fig. 9.- Weighted mean value of the Pb-Pb zircon ages for the dated samples. a) garnet-sillimanite-bearing gneiss (sample Su11d), b) enderbitic gneiss (sample Su3f), c) garnet-bearing gneiss (sample LC-57-2a), d) pegmatite layer (sample LC-57-2b). White bars - zircon not used for mean value calculation.

Fig. 9.- Valeur moyenne des âges Pb-Pb sur zircons des échantillons datés. a) gneiss à grenat-sillimanite (échantillon Su11d), b) gneiss enderbitique (échantillon Su3f), c) gneiss à grenat (échantillon LC-57-2a), d) intercalation de pegmatite (échantillon LC-57-2b). Barres blanches - zircons non utilisés pour le calcul d'âge moyen.

At BRGM, samples LC57-2a, Su3f and Su11d were analysed with a Finnigan MAT261 mass spectrometer following the experimental procedure described in Cocherie *et al*. (1992).

Each heating step took 4 - 5 minutes at the Belém laboratory and about 20 minutes at the Orléans laboratory. Weighted mean and corresponding errors on the ages were calculated according to Gaudette *et al*. (1998) for samples analysed at Belém and according to Ludwig (2001) for those analysed in Orléans; the errors on the mean age are quoted at a 2σ level. For all the samples, Pb-evaporation diagrams were drawn using the ISOPLOT program of Ludwig (2001).

Two samples of monazite were analysed by electron probe microanalyzer (EPMA), which enables high spatial-resolution dating together with systematic and detailed studies of small minerals. Like zircon, monazite records the complex history undergone by the host rocks. Therefore, it is of great interest to obtain ages under the best spatial-resolution conditions. After the pioneer studies of Suzuki and Adachi (1991), recent improvements in the statistical treatment of a large number of *in situ* data now make it possible to decipher the related thermal events, and so obtain reliable and precise ages (Cocherie and Albarède, 2001). In the case of monazites exhibiting significant Th/U ratio variation, data reduction in the Th/Pb = f(U/Pb) diagram

commonly allows a precision of ± 5-10 Ma to be achieved at the 2σ level (Cocherie *et al*., 2002). The use of both the ISOPLOT (Ludwig, 2001) and EPMA dating (Pommier *et al*., 2003) programs allows reduction of a statistically large number of data in a reproducible way.

Sm-Nd isotopic analyses of seven whole-rock samples (Su3f, Su10e1, Su10e2, Su11d, Su14a, Su14c and Su15) were carried out at the geochronological laboratory of the University of Brasília, Brazil, with isotopic measurements performed on a Finnigan MAT262 multicollector mass spectrometer in static mode using *double Re filaments*. The chemical separations of REE from other elements, and of Sm and Nd, are described in Gioia and Pimentel (2000). The mean $^{143}Nd/^{144}Nd$ values obtained on repeated analyses of the La Jolla standard during the studies were 0.511819 ± 17 (n=19, 1σm) and 0.511843 ± 24 (n=12, 2σ). Total blanks for Nd were about 90 pg. Nd T_{DM} model ages were calculated using the DePaolo (1981) model for depleted mantle evolution.

Pb isotopic data on zircons

The Pb isotopic results are presented in Table 4 and Figures 9 and 10.

Sample Su11d, a garnet-sillimanite-bearing gneiss, displayed two populations of zircon with distinct features. One population consists of clear, elongated, pink or transparent grains with preserved faces. The second population is composed of rounded multifaceted grains with typical features of metamorphic grains. Four grains from the latter population were analysed. Each grain behaved differently and furnished scattered results. Grain #A gave increasing age values at each step, up to 2106 Ma, with a mean value of 2097 ± 10 Ma for the three last steps (Fig. 9a). Grain #C provided four steps with similar ages and a mean value of 2072 ± 4 Ma. Crystal #D furnished a mean value of 2056 ± 14 Ma on two steps, and grain #F indicated an age of 2066 ± 8 Ma on one step. The mean value on the last three grains defined a poorly confident age of 2072 ± 4 Ma. Because of the metamorphic features of the zircons, the 2.07 Ga age is considered as the recrystallization age of the grains during high-grade metamorphism, and the older age obtained on grain A as indicating the existence of an inherited lead component with a minimum age of 2097 Ma.

Zircon	Temp. T°C	Number of ratios	206Pb/ 204Pb	208Pb/ 206Pb	207Pb*/ 206Pb*	σ	Age (Ma) step	2σ	Age (Ma) Grain	2σ
Metadolerite dyke - sample Su12aDF										
Su12aDF/1	*1450*	*18*	*11494*	*0.106*	*0.12421*	*54*	*2018*	*8*		
	1500	*82*	*166667*	*0.122*	*0.12663*	*18*	*2052*	*2*		
	1550	88	200000	0.160	0.12794	25	2070	3	2070	3
Su12aDF/2	*1450*	*96*	*142857*	*0.100*	*0.12479*	*37*	*2026*	*5*		
	1500	*96*	*500000*	*0.113*	*0.12595*	*30*	*2042*	*4*		
	1550	09	333333	0.129	0.12642	66	2049	9		
	1550	45	500000	0.130	0.12690	40	2056	6	2054	1
Su12aDF/3	*1450*	*18*	*14706*	*0.064*	*0.12206*	*54*	*1987*	*8*		
	1500	*54*	*71429*	*0.082*	*0.12452*	*26*	*2022*	*4*		
	1550	88	200000	0.117	0.12649	34	2050	5	2050	5
Su12aDF/4	*1450*	*70*	*142857*	*0.106*	*0.12452*	*22*	*2022*	*3*		
	1500	*90*	*250000*	*0.120*	*0.12591*	*16*	*2042*	*2*		
	1550	84	500000	0.124	0.12739	16	2063	2	2063	2
Su12aDF/5	*1450*	*12*	*8547*	*0.117*	*0.12334*	*117*	*2006*	*17*		
	1500	*88*	*500000*	*0.123*	*0.12646*	*17*	*2050*	*2*		
	1550	84	500000	0.141	0.12698	28	2057	4	2057	4
Su12aDF/6	1500	68	166667	0.120	0.12655	25	2051	3		
	1550	84	500000	0.129	0.12652	20	2051	3	2051	2
Su12aDF/7	*1450*	*68*	*5208*	*0.087*	*0.12469*	*34*	*2025*	*5*		
	1600	*97*	*142857*	*0.096*	*0.12476*	*35*	*2026*	*5*		
Su12aDF/8	*1500*	*18*	*> 1000000*	*0.077*	*0.12508*	*41*	*2030*	*6*		
	1550	*84*	*>1000000*	*0.111*	*0.12633*	*23*	*2048*	*3*		
	1600	88	>1000000	0.124	0.12709	20	2058	3	2058	3
	Mean (USD=4.0 - grains 1, 2, 3, 4, 5, 6):								2058	5
	Mean (USD=3.1 - grains 2, 3, 4, 5, 6):								2058	5
Metadolerite dyke - sample Su12aDV										
Su12aDV/1	*1450*	*90*	*333333*	*0.066*	*0.12282*	*39*	*1998*	*6*		
	1500	*86*	*500000*	*0.059*	*0.12536*	*19*	*2034*	*3*		
	1550	88	1000000	0.118	0.12687	18	2055	3		
	1560	88	>1000000	0.136	0.12709	40	2058	6	2056	2
Su12aDV/2	*1450*	*86*	*333333*	*0.099*	*0.12452*	*18*	*2022*	*3*		
	1500	*82*	*>1000000*	*0.125*	*0.12630*	*29*	*2047*	*4*		
	1550	86	>1000000	0.139	0.12707	31	2058	4	2058	4
Su12aDV/3	*1450*	*8*	*111111*	*0.103*	*0.12322*	*46*	*2004*	*7*		
	1500	*54*	*500000*	*0.108*	*0.12463*	*21*	*2024*	*3*		
	1550	*88*	*1000000*	*0.120*	*0.12489*	*28*	*2028*	*4*		
	1550	*80*	*250000*	*0.122*	*0.12521*	*19*	*2032*	*3*		
Su12aDV/4	*1450*	*54*	*23810*	*0.098*	*0.12308*	*30*	*2002*	*4*		
	1500	86	500000	0.141	0.12730	17	2061	2		
	1550	90	>1000000	0.160	0.12766	17	2066	2		
	1560	88	333333	0.135	0.12682	27	2055	4	2062	5
	Mean (USD = 3.1 - grains 1,2,4):								2060	4
Pegmatite (Sample Su15)										
Su15/01	*1450*	*45*	*16949*	*0.026*	*0.12092*	*54*	*1970*	*8*		
	1500	*49*	*62500*	*0.107*	*0.12472*	*23*	*2025*	*3*		
	1550	88	500000	0.168	0.12732	24	2062	3	2062	3
Su15/02	1450	18	> 1000000	0.072	0.12240	65	1992	9		
	1500	88	166667	0.071	0.12170	45	1982	7		
	1550	84	500000	0.073	0.12183	23	1984	3		
	1570	86	> 1000000	0.069	0.12173	23	1982	3	1983	2
Su15/03	*1450*	*10*	*15873*	*0.041*	*0.11900*	*230*	*1942*	*35*		
	1500	48	333333	0.046	0.12119	32	1974	5		
	1550	47	500000	0.046	0.12143	26	1978	4	1976	3
Su15/04	*1450*	*12*	*8621*	*0.064*	*0.12618*	*87*	*2046*	*12*		
	1500	*18*	*26316*	*0.105*	*0.12596*	*41*	*2043*	*6*		
	1550	48	52632	0.158	0.12677	50	2054	7		
	1570	19	15152	0.153	0.12705	69	2058	10	2055	6
Su15/05	*1450*	*34*	*12987*	*0.013*	*0.12800*	*31*	*2071*	*4*		
	1500	48	27027	0.013	0.12887	16	2083	2		
	1550	48	37037	0.013	0.12927	18	2088	2	2085	5
Su15/06	*1500*	*86*	*111111*	*0.094*	*0.12502*	*25*	*2029*	*4*		
	1550	90	200000	0.097	0.12701	20	2057	3	2057	3
Su15/07	1450	10	62500	0.009	0.12871	59	2081	8		
	1500	47	111111	0.012	0.12849	17	2078	2		
	1550	47	166667	0.008	0.12849	52	2078	7	2078	2
Su15/08	1450	84	83333	0.048	0.12788	24	2069	3		
	1500	90	100000	0.075	0.12802	30	2071	4		
	1550	84	250000	0.086	0.12820	26	2074	4	2071	3
	Mean (USD = 6.6 - grains 1, 4, 5, 6, 7, 8, 9):								2075	6
	Mean (USD = 2.0 - grains 2, 3):								1981	3
	Mean (USD = 1.4 - grains 1,4,6):								2059	3

Table 4.- Pb-evaporation isotopic results for the dated samples. Values in italics have not been included in the calculation of the age of the grain.

Tabl. 4.- Résultats isotopiques par évaporation de Pb pour les échantillons analysés. Les valeurs en italiques n'ont pas été incluses dans le calcul de l'âge du grain.

Garnet bearing gneiss - sample LC-57-2a

Zr A	1480	17	28300	0.034	0.12705	97	2058	26	**2058**	**26**
Zr B	*1440*	*45*	*62950*	*0.031*	*0.12390*	*46*	*2013*	*28*		
	1460	*60*	*251600*	*0.038*	*0.12562*	*15*	*2038*	*8*		
	1480	60	230720	0.039	0.12681	19	2054	6		
	1500	62	79600	0.038	0.12696	33	2056	10		
	1520	66	105720	0.037	0.12666	36	2052	10		
	1540	13	28530	0.034	0.12663	79	2052	22	**2054**	**10**
Zr C	1420	57	57960	0.032	0.12650	32	2050	8		
	1440	56	105270	0.034	0.12673	21	2053	6		
	1460	21	24940	0.032	0.12707	77	2058	22		
	1500	58	134910	0.030	0.12734	22	2062	6	**2055**	**8**
Zr D	*1400*	*26*	*10110*	*0.041*	*0.12545*	*42*	*2035*	*24*		
	Mean (MSWD = 0.9 - grains A, B, C)								**2055**	**3**

Pegmatite layer - Sample LC-57-2b

57-2B/1	*1500*	*86*	*20408*	*0.072*	*0.12563*	*18*	*2038*	*3*		
	1540	*88*	*5495*	*0.068*	*0.12665*	*40*	*2052*	*6*		
	1570	80	7092	0.055	0.12693	17	2056	2		
	1581	*32*	*45455*	*0.042*	*0.12848*	*49*	*2078*	*7*		
	1593	80	40000	0.055	0.12704	20	2058	3		
	1600	86	31250	0.047	0.12703	20	2058	3		
	1611	84	25641	0.041	0.12728	17	2061	2		
	1621	86	34483	0.037	0.12722	18	2060	3		
	1634	84	55556	0.034	0.12711	22	2059	3		
	1650	82	47619	0.033	0.12679	19	2054	3	**2058**	**2**
57-2B/2	*1520*	*90*	*35714*	*0.047*	*0.1264*	*23*	*2049*	*3*		
	1553	88	76923	0.033	0.12777	18	2068	2		
	1563	90	200000	0.029	0.12732	23	2062	3		
	1570	88	200000	0.028	0.12734	18	2062	3		
	1590	60	166667	0.028	0.12743	25	2063	3	**2064**	**3**
57-2B/3	*1480*	*34*	*3717*	*0.053*	*0.12661*	*36*	*2052*	*5*		
	1500	*82*	*23256*	*0.051*	*0.12708*	*24*	*2058*	*3*		
	1530	86	24390	0.043	0.12836	29	2076	4		
	1540	90	200000	0.038	0.12871	18	2081	2		
	1550	88	333333	0.034	0.12841	23	2077	3		
	1560	88	200000	0.033	0.12864	20	2080	3		
	1570	82	500000	0.031	0.12858	26	2079	4		
	1600	90	500000	0.031	0.12864	21	2080	3	**2079**	**1**
57-2B/4	*1480*	*18*	*6667*	*0.052*	*0.12532*	*56*	*2034*	*8*		
	1500	*50*	*6711*	*0.072*	*0.12529*	*45*	*2033*	*6*		
	1533	*90*	*7407*	*0.074*	*0.1264*	*32*	*2049*	*5*		
	1550	*82*	*23256*	*0.061*	*0.12739*	*21*	*2063*	*3*		
	1560	*88*	*58824*	*0.047*	*0.12729*	*20*	*2061*	*3*		
	1581	*16*	*58824*	*0.042*	*0.12809*	*38*	*2072*	*5*		
	1600	90	142857	0.033	0.12888	21	2083	3		
	1630	84	> 1000000	0.031	0.12906	33	2085	4		
	1650	70	31250	0.031	0.12879	51	2082	7	**2084**	**2**
57-2B/5	1510	54	> 1000000	0.034	0.12885	34	2083	5		
	1524	36	250000	0.034	0.12846	112	2077	15		
	1533	18	> 1000000	0.039	0.12833	101	2076	14		
	1541	18	> 1000000	0.036	0.12898	61	2084	8		
	1565	62	166667	0.034	0.12915	27	2087	4		
	1573	48	500000	0.032	0.12909	39	2086	5		
	1585	66	500000	0.031	0.12895	26	2084	4		
	1610	52	>1000000	0.030	0.12972	49	2095	7	**2085**	**3**
	Mean (USD = 7.0 - grains 1, 2, 3, 4, 5)								2069	4
	Mean (USD = 1.9 - grains 3, 4, 5)								2081	2

Enderbitic gneiss - Sample Su3f

ZRA	1520	65	22598	0.175	0.13255	53	2132	7	**2132**	**7**
ZRB	1520	67	9181	0.227	0.13415	31	2153	4	**2153**	**4**
ZRC	*1480*	*15*	*3353*	*0.193*	*0.12329*	*158*	*2047*	*22*		
	1560	*62*	*54127*	*0.146*	*0.12658*	*14*	*2051*	*2*		
	1600	*56*	*41008*	*0.098*	*0.12781*	*29*	*2068*	*4*		
	1640	*15*	*44110*	*0.095*	*0.12846*	*37*	*2077*	*5*		
	1640	*53*	*53857*	*0.096*	*0.12868*	*7*	*2080*	*1*		
	1680	66	36067	0.090	0.12919	22	2087	3		
	1680	36	16342	0.090	0.12883	44	2082	6	**2086**	**3**

Mylonitic charnockite - sample Su6b

Su6b/1	*1450*	*84*	*33333*	*0.115*	*0.12350*	*19*	*2008*	*3*		
	1480	*12*	*45455*	*0.152*	*0.12504*	*47*	*2030*	*7*		
	1520	*18*	*>1000000*	*0.198*	*0.12614*	*50*	*2045*	*7*		
	1560	52	26316	0.257	0.12715	27	2059	4	**2059**	**4**
Su6b/2	*1450*	*18*	*5376*	*0.212*	*0.12345*	*43*	*2007*	*6*		
	1500	*88*	*14925*	*0.265*	*0.12705*	*21*	*2058*	*3*		
	1530	*90*	*41667*	*0.281*	*0.12765*	*21*	*2066*	*3*		
	1560	54	14493	0.260	0.12780	34	2068	5	**2067**	**2**

Table 4.- Suite/Continued

Su6b/3	*1500*	*66*	*27778*	*0.240*	*0.12544*	*41*	*2035*	*6*	
Su6b/4	1500	52	>1000000	0.222	0.12795	46	2070	6	
	1550	16	>1000000	0.189	0.12793	51	2070	7	**2070** 5
Su6b/5	*1450*	*18*	*6757*	*0.246*	*0.12590*	*63*	*2042*	*9*	
	1485	88	16949	0.274	0.12727	25	2061	3	
	1550	86	52632	0.348	0.12780	28	2068	4	**2064** 7
Su6b/6	*1450*	*16*	*27778*	*0.095*	*0.12320*	*57*	*2003*	*8*	
	1500	*88*	*27778*	*0.129*	*0.12457*	*28*	*2023*	*4*	
	1520	90	14286	0.253	0.12712	26	2059	4	
	1550	78	40000	0.277	0.12753	24	2064	3	**2062** 6
Su6b/7	*1450*	*18*	*52632*	*0.175*	*0.12701*	*46*	*2057*	*6*	
	1500	*88*	*142857*	*0.122*	*0.12781*	*18*	*2068*	*3*	
	1520	*88*	*250000*	*0.070*	*0.12845*	*17*	*2077*	*2*	
	1550	*80*	*500000*	*0.070*	*0.12869*	*23*	*2080*	*3*	
	1560	*90*	*333333*	*0.066*	*0.12885*	*27*	*2083*	*4*	*2083* *4*
Su6b/8	*1450*	*50*	*9901*	*0.117*	*0.12691*	*55*	*2056*	*8*	
	1500	88	9259	0.064	0.12742	29	2063	4	**2063** 4
Su6b/9	*1450*	*80*	*31250*	*0.144*	*0.12405*	*19*	*2016*	*3*	
	1500	*90*	*16949*	*0.136*	*0.12512*	*24*	*2031*	*3*	
	1520	*80*	*10309*	*0.125*	*0.12538*	*43*	*2034*	*6*	
	1550	*86*	*5128*	*0.129*	*0.12466*	*43*	*2024*	*6*	
Su6b/11	*1450*	*84*	*34483*	*0.137*	*0.12728*	*17*	*2061*	*2*	
	1500	78	40000	0.119	0.12786	20	2069	3	
	1520	86	83333	0.244	0.12793	21	2070	3	
	1540	90	33333	0.139	0.12751	41	2064	6	**2069** 2
Su6b/12	*1450*	*84*	*14493*	*0.194*	*0.12393*	*22*	*2014*	*3*	
	1500	*86*	*38462*	*0.296*	*0.12634*	*20*	*2048*	*3*	
	1550	*54*	*10753*	*0.374*	*0.12665*	*39*	*2052*	*5*	
				Mean (USD=2.2 - grains 1, 2, 4, 5, 6, 8, 11, 12):					**2065** **2**
Sillimanite-garnet-bearing gneiss - sample Su11d									
ZRA	1560	16	8744	0.018	0.12839	191	2076	26	
	1600	21	5102	0.019	0.12963	179	2093	24	
	1640	29	15010	0.038	0.12941	118	2090	16	
	1680	15	40402	0.053	0.13060	120	2106	16	2097 10
ZRC	1500	12	9495	0.036	0.12781	44	2068	6	
	1520	17	10162	0.030	0.12766	58	2066	8	
	1560	56	24208	0.026	0.12795	15	2070	2	
	1580	61	64097	0.021	0.12831	15	2075	2	2072 4
ZRD	1480	22	4375	0.167	0.12723	131	2060	18	
	1480	15	10586	0.017	0.12658	144	2051	20	2056 14
ZRF	1440	37	4956	0.055	0.12766	58	2066	8	2066 8
				Mean (MSWD = 3.0 - grains C, D, F)					2072 4
Anorthosite - sample ER117									
ER117/01	*1460*	*16*	*> 1000000*	*0.221*	*0.12081*	*254*	*1969*	*38*	
	1480	54	> 1000000	0.237	0.12158	38	1980	6	
	1500	88	> 1000000	0.206	0.12113	22	1973	3	
	1540	90	1000000	0.163	0.12136	24	1977	4	
	1590	88	> 1000000	0.174	0.12123	19	1975	3	1975 2
ER117/02	1450	88	500000	0.100	0.12265	18	1995	3	
	1500	88	> 1000000	0.092	0.12231	30	1991	4	
	1550	18	> 1000000	0.095	0.12185	37	1984	5	1993 6
ER117/03	1450	49	1000000	0.150	0.12112	37	1973	6	
	1500	45	500000	0.167	0.12112	18	1973	3	1973 2
	1470	29	500000	0.155	0.12147	44	1978	6	
	1470	18	> 1000000	0.143	0.12306	104	2001	15	
	1470	52	> 1000000	0.122	0.12175	38	1982	6	1982 6
				Mean (USD = 4.5 - grains 1, 2, 3, 4)					1980 5

Zircons with $^{206}Pb/^{204}Pb$ < 2500 or with Pb signal too low during isotopic analyse are not shown in the table
Italic: step not included in the age calculation of the grain
*: radiogenic lead

Table 4.- Suite/Continued

Zircons from sample Su3f, an enderbitic gneiss, are very clear, rounded and pink. Only three grains were dated, which gave only one or two heating steps and furnished ages of 2153 ± 2 Ma, 2132 ± 3 Ma and 2087 ± 1 Ma (Fig. 9b). The wide range of values do not permit a confident age to be defined for this sample, but the results do indicate the presence of an inherited lead component, or of inherited zircons with ages older than those of the previous sample.

Zircons from sample LC57-2a, a garnet-bearing gneiss, are dark-brown with preserved prisms and rounded pyramids. Four grains were analysed, of which two (ZrA and ZrD) provided only one heating step and two (ZrB and ZrC) furnished four to six heating steps. The two latter grains show similar ages at four steps, which are also similar to the age of grain ZrA. The mean value calculated on the three grains gives an age of 2055 ± 3 Ma (mswd = 0.90), which corresponds to the crystallization or recrystallization age of the zircons (Fig. 9c).
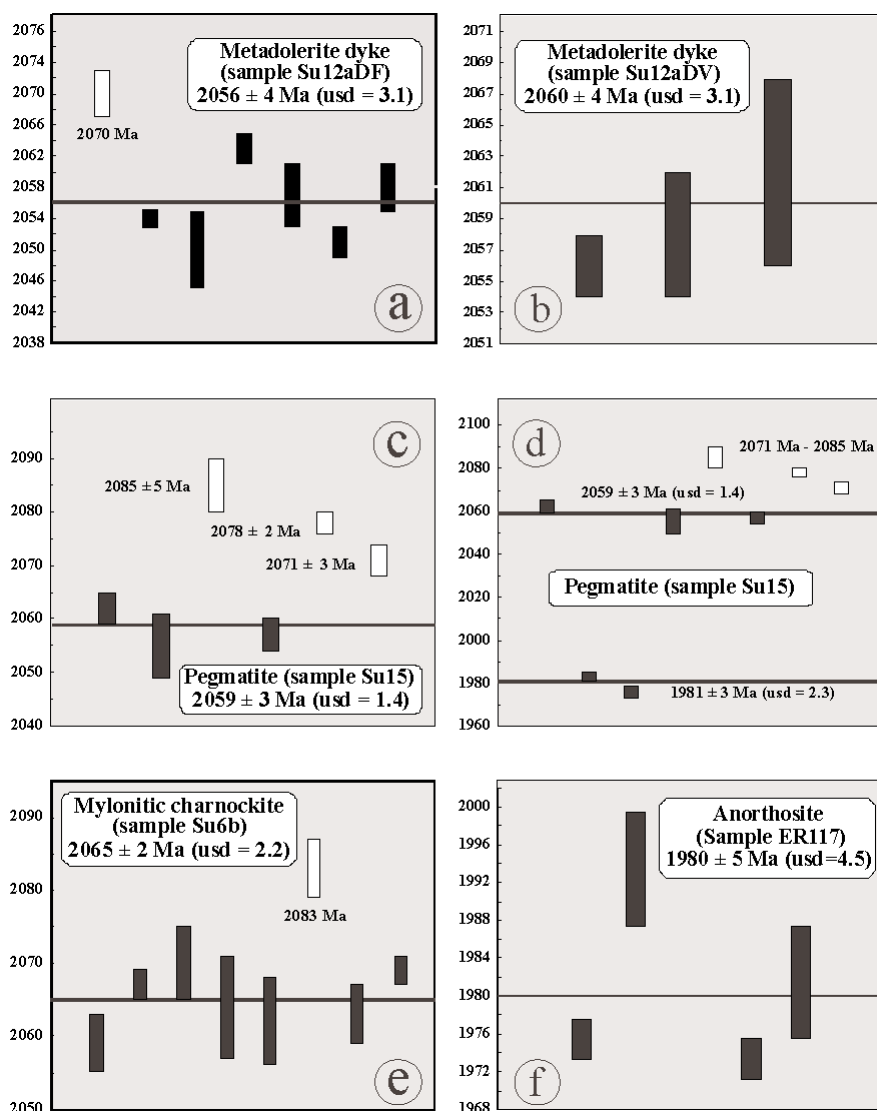
Fig. 10.- Weighted mean value of the Pb-Pb zircon ages for the dated samples. a) metadolerite dyke (sample Su12aDF), b) metadolerite dyke (sample Su12aDV), c) pegmatite (sample Su15), d) pegmatite (sample Su15), including the lower ages, e) mylonitic charnockite (sample Su6b), f) anorthosite (sample ER117). White bars - zircon not used for mean value calculation.

Fig. 10.- Valeur moyenne des âges Pb-Pb sur zircons des échantillons datés. a) dyke de métadolérite (échantillon Su12aDF), b) dyke de métadolérite (échantillon Su12aDV), c) pegmatite (échantillon Su15), d) pegmatite (échantillon Su15), incluant les âges les plus bas, e) charnockite mylonitique (échantillon Su6b), f) anorthosite (échantillon ER117). Barres blanches - zircons non utilisés pour le calcul d'âge moyen.

Sample LC57-2b, from a pegmatite layer within the previous sample (LC-57-2a), furnished a homogeneous population of very large sub-euhedral, stubby, brown and highly fractured zircons, much bigger than those of sample LC57-2a. No evidence of cores has been observed, but some of the grains display magmatic zoning. Five grains were dated, all of which furnished at least five temperature steps and, in some cases, up to 10 steps, probably due to the large size of the crystals. Each grain gave three or more heating steps with similar ages, but the ages varied significantly between 2085 ± 3 Ma and 2058 ± 2 Ma from one grain to another (Fig. 9d). The three older grains provided a mean value of 2081 ± 2 Ma, which could be interpreted as the age

of zircon crystallization during pegmatite emplacement. However, zircons from the country rock (LC57-2a) of the pegmatite furnished an age of 2055 Ma, which suggests that the value of about 2.08 Ga corresponds rather to the age of inherited zircon and that the ages of 2058 ± 2 Ma and 2064 ± 3 Ma correspond to a renewal of the U-Pb system in the other two crystals during pegmatite emplacement. As field relationships suggest that the pegmatite is the product of country rock melting, the existence of older zircons in the pegmatite implies that the age of 2055 ± 3 Ma obtained on gneiss sample LC-57-2a corresponds to a zircon recrystallization age with a total resetting of the U-Pb system during the high-grade episode. The older ages found in most of the zircon population from the pegmatite may be explained by the large size of the grains, which favours the preservation of the U-Pb system in internal domains, unaffected by melting.

Zircons from sample Su12aDF, a metadolerite dyke, are clear, elongated, euhedral to sub-euhedral crystals with fractures and inclusions. One grain (#10) is rounded with no preserved faces. Eight grains were analysed, all providing Pb at two heating steps, at least. In general, the lower temperature steps gave lower ages, except for grain #6. The mean value calculated on six grains furnished an age of 2056 ± 4 Ma (usd = 3.1), considered as the age of dyke crystallization (Fig. 10a). Grain #1 provided a slightly older age of 2070 ± 3 Ma, while grain #7 displayed a younger age of 2026 ± 5 Ma (not represented in Fig. 10a); these reflect an inherited lead component and lead loss, respectively, and both were discarded for the mean age calculation.

Zircons from sample Su12aDV, from the same metadolerite dyke, are sub-euhedral, clear, elongated to oval, with fractures and inclusions, i.e. similar to those of the previous sample. Four crystals were analysed. They gave three or more heating steps. The mean age determined from three grains was 2060 ± 4 Ma with usd = 3.1 (Fig. 10b). Grain #3, which displays a lower age, was not included in the mean age calculation. The 2060 ± 4 Ma age can be considered as

the age of zircon crystallization during the dyke emplacement, as with the previous sample.

Pegmatite sample Su15 provided clear, elongated, sub-euhedral zircons with preserved prisms and rounded pyramids. No evidence of zoning was observed. Two grains display distinct features from the main population. Grain #2 presents a clear, transparent, oval core surrounded by a thin-zoned mantle. Grain #3 is a clear, rounded, anhedral crystal without any visible internal structure, suggesting that it has been totally recrystallized. Eight grains were dated, most furnishing three or more heating steps. A wide range of ages between 1976 Ma and 2085 Ma was obtained; these are distributed in three groups (Fig. 10c and d). Crystals #5, 7 and 8 provided ages between 2071 Ma and 2085 Ma, while crystals #1, 4, and 6 gave a well-defined age at 2059 ± 3 Ma (usd = 1.4) and grains #2 and 3 furnished a mean age of 1981 ± 3 Ma (usd = 2.0). The 2059 ± 3 Ma age is interpreted as the age of pegmatite crystallization, and the older crystals may represent inherited zircons from an older source (>2085 Ma) of the pegmatite. No morphological difference can be seen between the 2.08 Ga and 2.06 Ga zircons. The age of 1981 ± 3 Ma obtained on the two recrystallized zircons may represent the overprinting by a younger event only identified in the anorthosite sample ER117 (see later), but the hypothesis that the age of 1.98 Ga may represent the emplacement age of the pegmatite and that the other two older ages may correspond to inherited lead component from source rocks cannot be totally discarded.

Sample Su06b from the mylonitic (magmatic) charnockite furnished two kinds of zircon, a population of rounded anhedral grains and a population of clear, elongated, euhedral crystals with a well-developed prism. Eleven grains were analyzed. Except for grain #3, a large number of heating steps was obtained and most of the grains gave a similar age at different steps. No correlation was established between the morphological features and the age of the zircons. Seven grains provided similar ages that define a mean value of 2065 ± 2 Ma (usd = 2.2), considered as the crystallization age of the zircons during charnockite emplacement (Fig. 10e). Three other grains furnished significantly lower ages and were discarded. Grain #7 displayed an increasing age, from 2057 Ma to 2083 Ma, at each heating step due to the contribution of an inherited lead component in the grain.

Only a few zircon grains were extracted from anorthosite sample ER117. Most are small, dark and anhedral, and no faces can be recognized. Fractures and inclusions are very abundant. Grain #2 displays different morphological features from the other crystals; its shape is oval, and corroded faces are distinguishable. Four grains were dated and furnished at least two steps with similar ages. The mean age calculated from the four grains was 1980 ± 5 Ma with usd = 4.5 (Fig. 10f). The high usd value indicates age variations probably due to small amounts of an inherited lead component in the crystals, as shown by grain #2. Despite this scattering, we consider the age of 1.98 Ga as a good approximation of the crystallization age of the zircons during anorthosite formation.

Microprobe lead data on monazite

The isotopic results from the microprobe Pb dating are presented in Table 5 and displayed in Figure 11.

Ten monazite grains (~100 µm) from a garnet-sillimanite-bearing gneiss (SU11d) were mounted in resin and polished to obtain cross sections. A detailed analytical procedure is given in Cocherie *et al*. (1998). Four of the 88 analyses were rejected statistically (2302 ± 145; 1805 ± 104; 1873 ± 139 and 1932 ± 119 Ma). The precision reached on the ages from each individual analysis is not very good (around ± 130 Ma), due to the rather low U and Th contents (Table 5). Nevertheless a relatively large spread of the data in the Th/Pb = f(U/Pb) diagram is observed (Fig. 11a). In addition, the regression line shows a slope similar to the two reference isochrons at 2200 and 2040 Ma, indicating that the regression line can be considered as an isochron and that, subsequently, an age can be calculated at the centroid of the population, where the age is more precisely defined. An age of 2127 ± 15 Ma is calculated using the data from all the studied grains. Another way to certify this age is to observe the age intercepts calculated on the two axes: these are identical, within the analytical errors (2116 ± 26 and 2234 +133-181 Ma). The age of 2127 Ma is interpreted as the crystallization age of the monazite.

Ten monazite grains (150 to 200 µm) from a leucogranitic layer (SU10e2) were also mounted in resin and polished to obtain cross sections. Back-scattered electron images show that nine of them comprise a large core surrounded by a
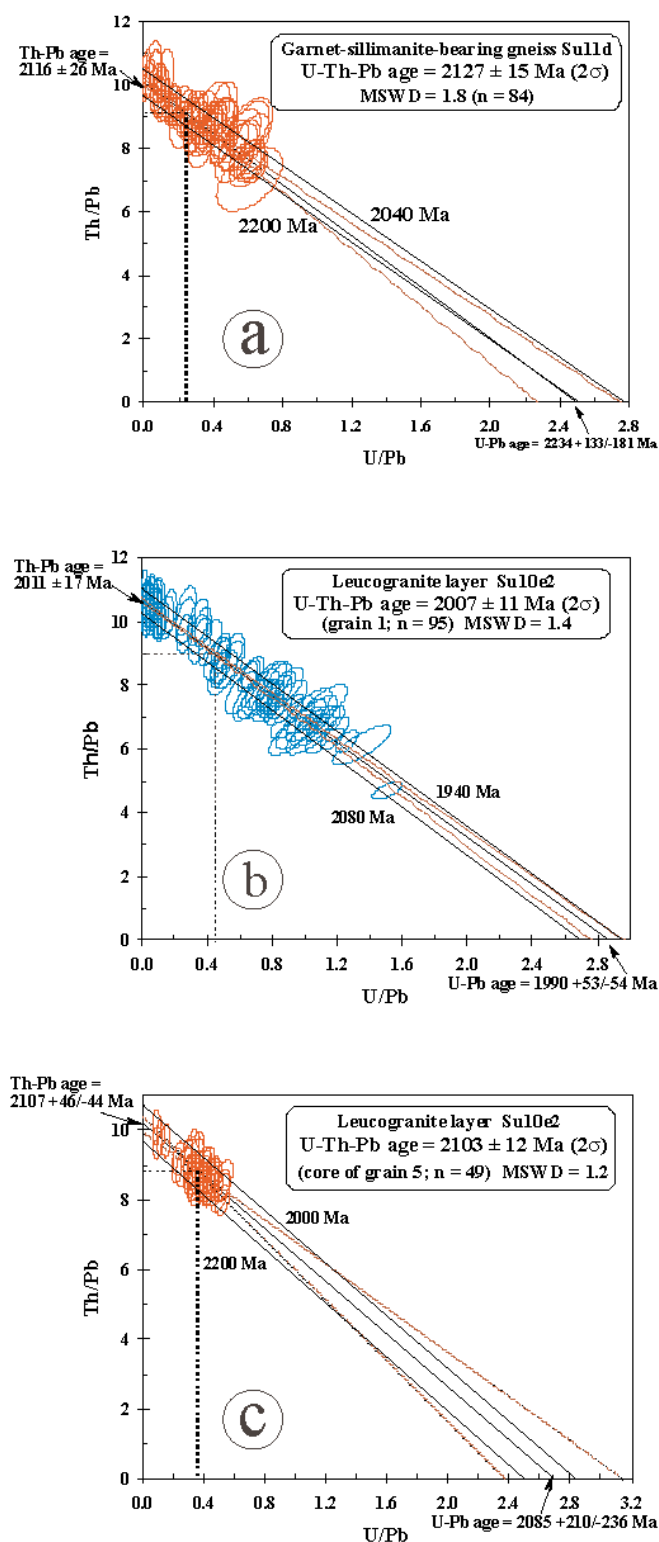
Pb (ppm) ± σ	U (ppm) ± σ	Th (ppm) ± σ	Isochron age ± 2σ Ma
Garnet-sillimanite- bearing gneiss Su11d			
4790±1783	1195±644	43742±19382	**2127±15** (n = 84)
leucogranite layer Su10e2			
Grain 1			
4897±1378	2176±2005	44203±17071	**2007±11** (n = 95)
Core of grain 5			
5667±778	2033±565	49956±8645	**2103±12** (n = 49)

Table 5.- Average electron microprobe analyses on monazite from samples Su10e2 and Su11d. Number of analyses considered are in brackets.

Tabl. 5.- Moyennes des analyses microsondes sur monazite pour les échantillons Su10e2 et Su11d. Le nombre d'analyses est indiqué entre parenthèses.

clearer rim related to a slightly higher Th content. The last grain appears to be more homogeneous and closer to the rim composition; it is labelled as "grain 1". Actually, as indicated in Table 5, both U and Th vary widely, giving a nice spread of the analyses in the Th/Pb = f(U/Pb) diagram (Fig. 11b). As observed on Figure 11b, numerous analyses are very close to the Th/Pb axis due to their high Th and low U content (7% Th and sometimes no detectable U). The slope of the regression line is exactly the same as that of the two reference isochrons at 2080 and 1940 Ma, indicating that the regression line can be considered as an isochron. An age of 2007 ± 11 Ma is calculated using all the 95 analyses from grain 1. Another way to confirm this age is to observe the age intercept calculated on the two axes at 2011 ± 17 and $1990 +53/-54$ Ma. The age of 2007 Ma is interpreted as the crystallization age of this monazite.

On the other side, the darker core of grain 5 has been extensively studied as being representative of the nine other monazites. The chemical composition is much more homogeneous, with around 5% Th and 2000 ppm U (Table 5). Despite the limited variation of Th/U ratio, a regression line can be drawn whose slope is parallel to the reference isochron (Fig. 11c). An average age of 2103 ± 12 Ma was calculated at the centroid of the population. Because these two ages seem to be related to two types of mineralogical domain, associated with distinct chemical compositions, we interpret the old age as an inherited age. The young age should represent the age of formation of the leucogranite layer; however, geological evidence points to a formation of this layer by syntectonic *in situ* melting during the granulitic event at 2.07-2.05 Ga. Consequently, the 2.0 Ga age is better interpreted as a resetting age during the late thermal event associated with anorthosite at 1.98 Ga. Like zircon, monazite can remain a closed system while the rock is subjected to high temperature, such as that associated with the migmatization (Cocherie *et al.*, 2000).

Sm-Nd isotopic data

The Sm-Nd results are displayed in Table 6, which also includes initial ε_{Nd} values calculated at the estimated formation age provided by Pb evaporation. Nd evolution lines for the samples have been plotted in the ε_{Nd} versus time diagram (Fig. 12). Apart from sample Su12c, which has a high $^{147}Sm/^{144}Nd$ ratio of 0.1634, all the samples showed $^{147}Sm/^{144}Nd$ in the range of 0.132 - 0.075, which makes the data useful for model age calculation. The samples gave Nd T_{DM} model ages from 2.19 Ga to 2.40 Ga, with $\varepsilon_{Nd(t)}$ between +1.43 and -0.37. The range of T_{DM} model ages, together with positive to slightly negative $\varepsilon_{Nd(t)}$ values, strongly suggest a short crustal residence time. Therefore, the precursors of the granulitic rocks from Bakhuis Mountains must have been formed during an eo-Transamazonian event of crustal differentiation from mantle, with minor participation of older crustal material (Fig. 12).

Fig. 11.- Th/Pb - U/Pb diagrams for monazite from the dated samples. a) Th/Pb = f(U/Pb) plot for 84 spot analyses from 10 monazite grains from garnet-sillimanite-bearing gneiss Su11d, b) Th/Pb = f(U/Pb) plot for 95 spot analyses from homogeneous monazite grain 1 from leucogranite layer Su10e2, c) Th/Pb = f(U/Pb) plot for 49 spot analyses from the core of monazite grain 5 from leucogranite layer Su10e2.

Fig. 11.- Diagrammes Th/Pb - U/Pb pour les monazites des échantillons datés a) report Th/Pb = f(U/Pb) pour 84 analyses effectuées sur 10 grains de monazite du gneiss à grenat-sillimanite Su11d, b) report Th/Pb = f(U/Pb) pour 95 analyses du grain de monazite homogène 1 de l'intercalation de leucogranite Su10e2, c) report Th/Pb = f(U/Pb) pour 49 analyses du cœur du grain de monazite 5 de l'intercalation de leucogranite Su10e2.

Sample	Rock type	Sm $_{ppm}$	Nd $_{ppm}$	$^{147}Sm/^{144}Nd$	1σ $(.10^{-4})$	$^{143}Nd/^{144}Nd$	1σ $(.10^{-6})$	$\varepsilon_{Nd(t)}$	$\varepsilon_{Nd(0)}$	T_{DM} (Ga)
Su 14c	pegmatite	39.14	180	0.1315	13	0.511762	11	0.16	-17.09	2.39
Su 12c	enderbitic gneiss	2.45	9.12	0.1634	16	0.512209	24	0.44	-8.37	-
Su 15	pegmatite	0.14	1.09	0.0750	8	0.511060	54	1.43	-30.78	2.19
Su 10e1	leucogranite layer	0.45	3.50	0.0788	8	0.511036	29	-0.06	-31.25	2.28
Su 14a	pegmatite	36.50	167	0.1318	13	0.511759	11	0.03	-17.15	2.40
Su 10e2	leucogranite layer	6.03	37.04	0.0984	10	0.511330	9	0.62	-25.52	2.27
Su11 d	gt-sill-bearing gneiss	3.73	21.09	0.1068	11	0.511404	9	-0.17	-24.07	2.35
Su3 f	enderbitic gneiss	4.10	20.76	0.1193	12	0.511564	9	-0.37	-20.95	2.40

Table 6.- Sm-Nd isotopic results for the dated samples. T_{DM} ages are calculated using the model of DePaolo (1981) for Nd evolution of the depleted mantle. Zircon Pb/Pb ages, when available, have been used for calculation of the $\varepsilon_{(Nd)}$ at T.

Tabl. 6.- Résultats isotopiques Sm-Nd des échantillons analysés. Les âges modèles T_{DM} ont été calculés selon le modèle de DePaolo (1981) pour l'évolution du Néodyme dans le manteau appauvri. Les âges zircons disponibles ont été utilisés pour le calcul de la valeur initiale $\varepsilon_{(Nd)}$.

Discussion of the isotopic results

Most of the zircon data are within the range 2085 - 2055 Ma, with dominant ages at 2065 - 2055 Ma, indicating a late-Transamazonian age for the high-grade metamorphism. This age is well constrained by the samples of metadolerite dyke (Su12aDV) and garnet-bearing gneiss (LC57-2a), which furnished ages around 2060 - 2055 Ma in all the dated grains, and by another sample of the metadolerite dyke (Su12aDF) which yielded ages of 2065 - 2056 Ma with one older grain at about 2070 Ma. Two pegmatite samples (Su15 and LC57-2b) provided more complex Pb-Pb zircon age patterns from 2058 Ma up to 2.09 - 2.08 Ga. Such a behaviour suggests that the rocks may have suffered the high-grade metamorphic event at around 2.09 - 2.07 Ga, followed by a melting event at 2065 - 2055 Ma. Alternatively, if we take into account only the confident zircon data that provide well-defined ages, the range of ages between 2072 Ma and 2055 Ma may represent a protracted (*ca.* 15-20 Ma) episode of high-grade metamorphism, which ended with partial melting of the country rock and pegmatite emplacement. The limitation of the Pb-evaporation method, which provides only $^{207}Pb/^{206}Pb$ ages and avoids the evaluation of the degree of discordance, plus the lack of internal structure and microchemistry studies of the grains, preclude any attempt to decipher the detailed chronology of metamorphic paths between 2080 and 2055 Ma.

The existence of rocks older than 2.08 Ga, up to 2.15 Ga, is indicated by the presence of an inherited lead component in zircons from an enderbitic gneiss and a garnet-sillimanite gneiss.

The 2065 Ma age of the mylonitic charnockite (Su6b) is striking. The rock is identical to the orthopyroxene granite (magmatic charnockite) that is so common in the southwestern part of the Bakhuis belt, but is rather rare in the core and northeastern part. The age shows that the granulite-facies metamorphism coincided with the local production of orthopyroxene granite.

Dating of zircons for the anorthosite ER117 provided the first evidence of a thermal pulse around 1.98 Ga. The existence of this younger event is also suggested by the age of about 1.98 Ga obtained on two zircons from pegmatite Su15.

Monazite appears, for the U-Th-Pb system, to be a reservoir as robust as zircon, because the oldest ages obtained on zircon in rocks from the region are also obtained on monazite - 2103 Ma for monazite of the garnet-sillimanite-bearing gneiss Su11d, and 2127 Ma for monazite of the leucogranite layer Su10e2. The age of 2103 Ma for monazite of Su11d is similar to the age of 2097 Ma obtained on one zircon, while all the other zircon crystals of the sample yielded an age of about 2.07 Ga, considered as the age of metamorphism. Moreover, most of the Pb-Pb ages furnished by zircons from the pegmatite layers and veins associated with the high-grade metamorphic rocks, were between 2080 and 2055 Ma, significantly younger than the age of 2127 Ma obtained on monazite of leucogranite layer Su10e2. However, monazite from that sample also registered a much younger thermal event around 2007 Ma, which may correspond to the magmatic pulse at about 1.98 Ga. Surprisingly, the U-Th-Pb system of monazite did not record the effect of the high-grade metamorphic event.

No evidence of an Archean inherited component has yet been detected in any zircon from the dated samples. The Sm-Nd results also indicate a lack of reworked Archean crust in
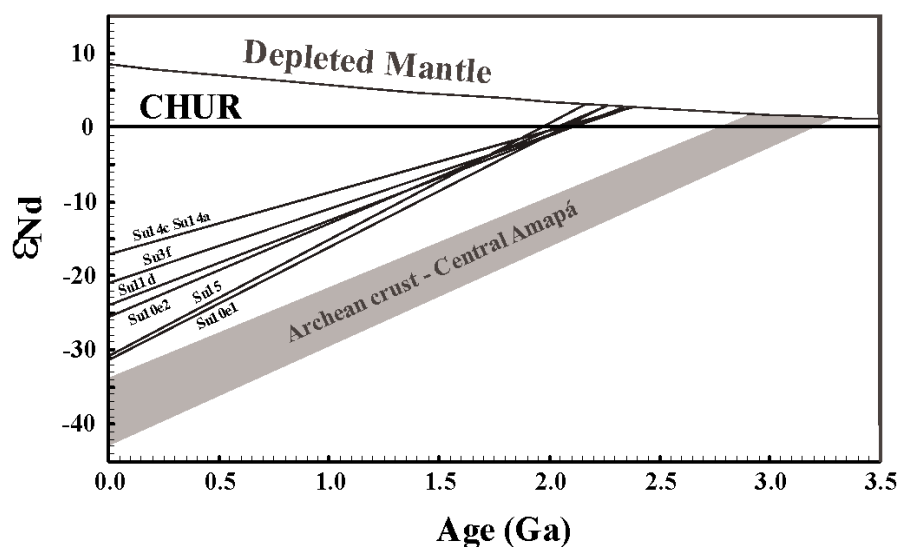
Fig. 12.- ε_{Nd} *versus* time diagram for the dated samples. The ε_{Nd} evolution line for the Archean crust of central Amapá is also shown in the diagram.

Fig. 12.- *Diagramme ε_{Nd} versus temps pour les échantillons datés. La courbe d'évolution ε_{Nd} concernant la croûte archéenne d'Amapá central est représentée aussi dans le diagramme.*

the Bakhuis Mountains, and point to a main episode of Paleoproterozoic juvenile crustal accretion during eo-Transamazonian times. These results are in good agreement with the U-Pb data and a previous whole-rock Sm-Nd result in the region (Priem *et al.*, 1978; Ben Othman *et al.*, 1984).

Discussion

The Bakhuis metamorphic rocks underwent UHT and near-UHT metamorphism. The extreme temperatures, between 900 and 1000 °C, require an extraordinary thermal regime and heat source. The counterclockwise P-T path of the prograde metamorphism found here, is often interpreted to have formed in and beneath areas of voluminous magmatic accretion (Harley, 1989; Waters, 1991), with or without additional crustal extension. The dating of an orthopyroxene granite (magmatic charnockite) showed that the generation of this granite was coeval with the UHT metamorphism. The charnockitic magmatism has only been found locally in the core of the Bakhuis belt, but voluminous orthopyroxene granite to tonalite bodies are present in the southwestern part of the belt outside the core. The rarity of such rocks in the core and their abundant presence in the southwestern part of the belt (with only scattered areas of pelitic gneiss and banded rocks of the charnockite suite) suggest that the southwestern area may represent a shallower part of the belt. This, in turn, may imply that the banded rocks of the charnockite suite in the core of the belt indeed occupied a position beneath a zone of voluminous magmatic accretion during UHT and near-UHT metamorphism.

Evidence of deep-seated magmatism as a possible driving process is present in the Bakhuis belt, although voluminous basic magmatism is found only in the southwestern part and is younger than the granulite-facies metamorphism.

Metadolerite (pyroxene amphibolite) dykes are widespread throughout the core of the Bakhuis belt. Some are partly synkinematic with the folding, but most are postkinematic, but nevertheless metamorphosed under granulite-facies conditions. Their widespread presence and formation during the granulite-facies metamorphism may be regarded as a special characteristic of the Bakhuis belt metamorphism. Zircon dating of a dyke indicated that the basic magmatism and granulite-facies metamorphism were contemporaneous.

Zircon dating of a rather large anorthosite body found in the core of the Bakhuis Mountains, showed that the anorthosite intruded the banded rocks of the charnockite suite at around 1.98 Ga, after the peak metamorphism and deformation at 2072 - 2055 Ma.

A still younger stage of deep-seated magmatic activity is represented by the gabbroic-ultramafic intrusions in the Bakhuis horst. They are quite abundant in the southwestern part of the belt but also occur outside of the belt.

The available evidence suggests that the high-grade rocks spent a long period at depth before exhumation. The age of the anorthosite body intrusive in the core of the belt indicates that the dome structure of the belt was formed considerably later than the peak metamorphism. The subvertical position of the magmatic layering in the anorthosite body strongly suggests intrusion before (or possibly during the initial stages of) the doming of the Bakhuis high-grade rocks. This would imply that the high-grade rocks, when intruded by the anorthosite body at around 1.98 Ga, were still at the deep crustal level where they had undergone granulite-facies metamorphism.

A large pyroxene granite body in the northeastern part of the Bakhuis belt was dated by Rb-Sr at 1923 ± 55 Ma (Priem, pers. comm.; isochron on drill-cores). This granite was probably intruded after the doming of the belt, because it resembles pyroxene granite and biotite granite occurring outside the belt, and because it lacks the catazonal characteristics of the (probably older) orthopyroxene granite to tonalite in the southwestern part of the belt, which contain abundant orthopyroxene and antiperthite. Doming probably occurred before or during the initial stages of the widespread granitic magmatism in northwestern Suriname that occurred

around this time. In southwestern Suriname, the Coeroeni gneiss was intruded like a migmatite massif in a highly mobile state into the surrounding crust (Kroonenberg, 1976), probably during the same period. Doming of the Bakhuis belt at least predated the cratonization of the Guiana Shield and the onset of Roraima Group sedimentation, at about 1875 Ma (Santos *et al.*, 2003).

Limited further exhumation occurred during the formation of the Bakhuis horst, which was due to the Nickerie metamorphic event at about 1200 Ma, and also during small later horst movements. The horst is bordered by mylonite zones, with ultramylonite and even pseudotachylite and tachylite. It is most probable that these late brittle to brittle-ductile tectonic features developed preferentially along pre-existing Transamazonian discontinuities. The mylonitization was accompanied by widespread Rb-Sr and K-Ar resetting of micas in the high-grade metamorphic and surrounding rocks, and by local low-grade metamorphism.

It is clear from this slow and long exhumation path that the retrograde metamorphism was probably complex and that finding a match will require more detailed study.

Conclusions

This study brings new results on both the petrological and the isotopic aspects of the Bakhuis granulite belt formation:

- Locally the granulite-facies metamorphism of the belt reached UHT conditions, with T as high as 950 °C and P around 8½-9 kb.

- The UHT metamorphism occurred under oxidizing conditions, as shown by the incorporation of Fe^{3+} in sillimanite, sapphirine and orthopyroxene, by the widespread formation of Fe oxide and spinel (probably forming a spinel solid solution at high T) and by the absence of garnet.

- The remainder of the core of the Bakhuis belt was probably metamorphosed at granulite-facies conditions near resp. not far from the UHT conditions. Possible remnants of UHT metamorphism have been found in at least two other locations. This suggests that the UHT metamorphism may have been more widespread, even though it cannot be recognised in part of the rocks and has been obliterated by retrograde metamorphism and mylonitization in other rocks.

- Petrological arguments suggest an early assemblage with cordierite + sillimanite, followed by an assemblage with sapphirine + quartz, and finally a peak assemblage orthopyroxene + sillimanite + quartz in the UHT occurrence. This points to a counterclockwise P-T path for the prograde metamorphism, going first toward higher temperature conditions, then to lower temperature conditions, with over-all some increase in pressure.

- The UHT metamorphism was coeval with the local production of true magmatic charnockite. The abundant presence of such charnockite in the southwestern part of the belt may suggest that the UHT metamorphism occurred below a zone of voluminous magmatic accretion.

- Retrograde metamorphism in the UHT occurrence is indicated, for example, by a marked reduction of the Al_2O_3 level from core to rim in the orthopyroxene, corresponding to an isobaric or near isobaric cooling (IBC) path.

From an isotopic point of view, zircon data on granulite are within the range of 2085 – 2055 Ma, with dominant ages at 2065 - 2055 Ma, indicating a late-Transamazonian age for the high-grade metamorphism. This can be interpreted either as a high-grade metamorphic event at around 2.07 - 2.09 Ga, followed by a melting event at 2065 - 2055 Ma, or alternatively may represent a protracted (*ca*. 15-20 Ma) episode of high-grade metamorphism, between 2072 Ma and 2055 Ma, which ended with partial melting of the country rocks and pegmatite emplacement, and locally even with full melting and the production of orthopyroxene granite. The existence of rocks older than 2.07 Ga, up to 2.15 Ga, is indicated by the presence of an inherited lead component in zircons from an enderbitic gneiss and a garnet-sillimanite gneiss. Dating of zircons from an anorthosite provides the first evidence of a thermal pulse around 1.98 Ga. The existence of a younger event at 1.98 Ga is also supported by Pb-Pb ages on zircons from a pegmatite.

Monazite appears, for the U-Th-Pb system, to be a reservoir as robust as zircon, because the oldest ages obtained on zircon in rocks from the region are also obtained on monazite. In addition, monazite from a leucogranite layer has registered a much younger thermal event around 2007 Ma, which may correspond to the magmatic pulse at about 1.98 Ga. Surprisingly, the U-Th-Pb system of monazite did not record the effect of the high-grade metamorphic event.

The Sm-Nd results also indicate a lack of reworked Archean crust in the Bakhuis Mountains, and point to a main episode of Paleoproterozoic juvenile crustal accretion during eo-Transamazonian times. These results are in good agreement with the U-Pb results and a previous whole-rock Sm-Nd result in the region (Priem *et al.* 1978; Ben Othman *et al.*, 1984).

Finally, we interpret the formation of the Bakhuis granulite belt, along with its UHT metamorphism, counterclockwise P-T path and coinciding charnockite magmatism, as the result of a major thermal perturbation. Moreover, we interpret this anomalous thermal pulse in terms of mantle advection at the base of the Transamazonian

crust at 2.07 - 2.05 Ga (indicated by contemporaneous basic dykes) and possibly continuing until *ca*. 2.0 Ga (as registered by anorthosite and local younger ages in the granulite). The global interpretation at Shield scale and regional correlations with adjoining domains have been given by Delor *et al.* (2001), and are the subject of a companion paper (Delor *et al.*, 2003) in which late-Transamazonian crustal stretching is proposed in the light of our conclusions on the petrological and isotopic data from the Bakhuis belt.

Acknowledgements

References

Arima M., Kerrich R., Thomas A. (1986) - Sapphirine-bearing paragneiss from the northern Grenville province in Labrador, Canada: protolith composition and metamorphic P-T conditions. *Geology*, **14**, 844-847.

Avelar V.G. de (2002) - Geocronologia Pb-Pb em zircão e Sm-Nd em rocha total da porção centro-norte do Estado do Amapá – Brasil: implicações para a evolução do setor oriental do Escudo das Guianas. Doctoral thesis, CPGG-UFPA, Belém, 212 p.

Avelar V.G. de, Lafon J.M., Delor C. (2001) - Geocronologia Pb-Pb em zircão e Sm-Nd em rocha total da porção centro-norte do Amapá. Implicações para a evolução geodinâmica do Escudo das Guianas. *In*: VII Simpósio de Geologia da Amazônia, Belém, SBG-NO. Resumos Expandidos (CD-ROM).

Avelar V.G. de, Lafon J.M., Delor C., Guerrot C., Lahondère D. (2003) - Archean crustal remnants in the easternmost part of the Guiana Shield: Pb-Pb and Sm-Nd geochronological evidence for Mesoarchean versus Neoarchean signatures. *Géologie de la France*, **2-3-4,** 83-99.

Baba S. (2003) - Two stages of sapphirine formation during prograde and retrograde metamorphism in the Paleoproterozoic Lewisian complex in south Harris, NW Scotland. *J. Petr.*, **44**, 329-354.

Bartlett J.M., Dougherty-Page J.S., Harris N.B.W., Hawkesworth C.J., Santosh M. (1998) - The application of single zircon evaporation and model Nd ages to the interpretation of polymetamorphic terrains: an example from the Proterozoic mobile belt of south India. *Contrib. Mineral. Petrol.*, **131** (2-3), 181-195.

Ben Othman D., Polvé M., Allegre C.J. (1984) - Nd-Sr isotopic composition of granulites and constraints on the evolution of the lower continental crust. *Nature*, **307**, 510-515.

Berrange J.P. (1977) - The geology of southern Guyana, South America. Inst. Geol. Sciences, London, Overseas Division, Memoir 4, 112 p.

Bose S., Fukuoka M., Sengupta P., Dasgupta S. (2000) - Evolution of high-Mg-Al granulites from Sunkarametta, eastern Ghats, India: evidence for a lower crustal heating-cooling trajectory. *J. Metamorph. Geol.*, **18**, 223-240.

Bosma W., Kroonenberg S.B., van Lissa R.V., Maas K., Roever E.W.F. de (1978) - Geological map of Suriname 1:500 000. Geol. Mijnb. Dienst Suriname.

Bosma W., Kroonenberg S.B., Maas K., Roever E.W.F. de (1983) - Igneous and metamorphic complexes of the Guiana Shield in Surinam. *Geol. Mijnbouw*, **62**, 241-254. (see also more extensive version *in: Geol. Mijnb. Dienst Sur., Med*. 27, 31-82).

Carrington D.P., Harley S.L. (1995) - Partial melting and phase relations in high-grade metapelites: an experimental petrogenetic grid in the KFMASH system. *Contrib. Mineral. Petrol.*, **120**, 270-291.

Cocherie A., Albarède F. (2001) - An improved U-Th-Pb age calculation for electron microprobe dating of monazite. *Geochim. Cosmochim. Acta,* **65**, 4509-4522.

Cocherie A., Guerrot C., Rossi Ph. (1992) - Single-zircon dating by step-wise evaporation: Comparison with other geochronological techniques applied to the Hercynian granites of Corsica, France. *Chemical Geology* (Isotope Geosciences Section), **101**, 131-141.

Cocherie A., Legendre O., Peucat J.J., Kouamelan A.N. (1998) - Geochronology of polygenetic monazites constained by *in situ* electron microprobe Th-U-total Pb determination: Implications for lead behaviour in monazite. *Geochim. Cosmochim. Acta*, **62**, 2475-2497.

Cocherie A., Rossi Ph., Legendre O., Lafon J.M., Delor C., Jezequel P. (2000) - Systematic dating on monazite and zircon by EPMA, a tool for geochronological surveying and mapping of Precambrian basements: the example of French Guiana. 31st Intern. Geol. Cong., Rio de Janeiro, Brazil, August 6-17, 2000.

Cocherie A., Be E., Legendre O., Fanning C.M. (2002) - Electron microprobe dating as a tool for understanding closure of the U-Th-Pb system in monazite: examples from migmatite. GSA 2002 Denver Annual Meeting (October 27-30, 2002), Abstracts, p. 172.

Dahlberg E.H. (1973) - Lithostratigraphical correlation of granulite-facies rocks of the Guiana Shield. Secondo Congreso Latino-Americano, Caracas, Venezuela. Also, *Geol. Mijnb. Dienst Sur.*, Med **23**, 26-33.

Das K., Dasgupta S., Miura H. (2003) - An experimentally constrained petrogenetic grid in the silica-saturated portion of the system KFMASH at high temperatures and pressures. *J. Petrol.*, **44**, 1055-1075.

Dasgupta S., Ehl J. (1993) – Reaction textures in a spinel-sapphirine granulite from the Eastern Ghats, India, and their implications. *Eur. J. Min.*, **5**, 537-543.

Dasgupta S., Sengupta P., Ehl J., Raith M., Bardhan S. (1995) - Reaction textures in a suite of spinel granulites from the Eastern Ghats belt, India: Evidence for polymetamorphism, a partial Petrogenetic grid in the system KFMASH and the roles of ZnO and Fe_2O_3. *J. Petrol.*, **36**, 435-461.

Delor C., Lafon J.M., Lahondère D., Roever E.W.F. de, Fraga M.L., Rossi P. (2001) - Paleoproterozoic framework of the Guiana Shield II - continental scale boudinage and ultra-high temperature granulite belt exhumation at 2.07-2.06 Ga. *In*: VII Simpósio de Geologia da Amazônia, Belém, SBG-NO. Resumos Expandidos (CD-ROM).

Delor C., Roever E.W.F. de, Lafon J.M., Lahondère D., Rossi P., Cocherie A., Guerrot C., Potrel A. (2003) - The Bakhuis ultrahigh-temperature granulite belt: II. implications for late Transamazonian crustal stretching in a revised Guiana Shield framework. *Géologie de la France,* **2-3-4**, 207-230.

DePaolo D.J. (1981) - A neodymium and strontium isotopic study of the Mesozoic calc-alkaline granitic batholiths of the Sierra Nevada and Peninsular Ranges, California. *J. Geophys. Res.*, **86**(B11),10470-10488.

Dougan T.W. (1974) - Cordierite gneisses and associated lithologies of the Guri area, northwest Guyana shield, Venezuela. *Contrib. Mineral. Petrol.,* **46**, 317-342.

Ellis D.J., Sheraton J.W., England R.N., Dallwitz W.B. (1980) - Osumilite-sapphirine-quartz granulites from Enderby Land, Antarctica - Mineral assemblages and reactions. *Contrib. Mineral. Petrol.*, **72**, 123-143.

Gaudette H.E., Lafon J.M., Macambira M.J.B., Moura C.A.V., Scheller T. (1998) - Comparison of single filament Pb evaporation/ionization zircon ages with conventional U-Pb results: examples from the Pre-Cambrian of Brazil. *J. South Amer. Earth Sci.*, **11**(4), 351-363.

Gibbs A.K., Barron C.N. (1993) - The geology of the Guyana Shield. Oxford University Press (New York); Clarendon Press (Oxford). Oxford Monographs on Geology and Geophysics, 22, 246 p.

Gioia S.M.C.L., Pimentel M.M. (2000) - The Sm-Nd isotopic method in the geochronology laboratory of the University of Brasília. *An. Acad. Bras.*, **72**, 220-245.

Guiraud M., Kienast J.-R., Ouzegane K. (1996) - Corundum-quartz-bearing assemblages in the Ihouhaouene area (in Ouzzal, Algeria). *J. Metamorph. Geol.*, **14**, 755-761.

Harley S.L. (1989) - The origins of granulites: a metamorphic perspective. *Geol. Mag.*, **126**, 215-247.

Harley S.L. (1998) - On the occurrence and characterization of ultrahigh-temperature crustal metamorphism. *In:* Treloar P.J., O'Brien P.J. (eds.) What drives metamorphism and metamorphic reactions? *Geol. Soc. Spec. Publ.*, **138**, 81-107.

Harley S.L., Sheraton J.W. (1990) - Two-stage decompression in orthopyroxene-sillimanite granulites from Forefinger point, Enderby Land, Antarctica: implications for the evolution of the Archaean Napier Complex. *J. Metamorph. Geol.*, **8**, 591-613.

Harlov D.E., Newton R.C. (1993) - Reversal of the metastable kyanite+corundum+quartz and andalusite+corundum+quartz equilibria and the enthalpy of formation of kyanite and andalusite. *Amer. Min.*, **78**, 594-600.

Harlov D.E., Milke R. (2002) - Stability of corundum+quartz relative to kyanite and sillimanite at high temperature and pressure. *Amer. Min.*, **87**, 424-432.

Hensen B.J. (1986) - Theoretical phase relations involving cordierite and garnet revisited: the influence of oxygen fugacity on the stability of sapphirine and spinel in the system Mg-Fe-Al-Si-O. *Contrib. Mineral. Petrol.*, **92**, 362-367.

Hensen B.J., Harley S.L. (1990) - Graphical analysis of P-T-X relations in granulite-facies metapelites. *In:* Ashworth J.R., Brown M. (eds.) High Temperature Metamorphism and Crustal anatexis. Unwin Hyman, London, 19-56.

Hood P., Tyl I. (1973) - Residual magnetic anomaly map of Guyana and its regional geological interpretation. Preprint 2nd Latin-American Geol. Congress, Caracas, Venezuela.

Jaeckel P., Kröner A., Kamo S.L., Brandl G., Wendt J.I. (1997) - Late Archean to early Proterozoic granitoid magmatism and high-grade metamorphism in the central Limpopo belt, South Africa. *J. Geol. Soc., London*, **154**, 25-44.

João X.S.J., Marinho P.A.C. (1982) - Catametamorfitos Arqueanos da região centro-leste do Território Federal do Amapá. *In:* Simp. Geol. Amaz. 1, Belem. Anais.. Belem. SBG. Vol. 2, 207-228.

Kober B. (1986) - Whole-grain evaporation for $^{207}Pb/^{206}Pb$-age-investigations on single zircons using a double-filament thermal ion source. *Contrib. Mineral. Petrol.*, **93**, 482-490.

Kober B. (1987) - Single zircon evaporation combined with Pb+ emitter-bedding for $^{207}Pb/^{206}Pb$-age investigations using thermal ion mass spectrometry, and implications to zirconology. *Contrib. Mineral. Petrol.*, **96**, 63-71.

Kouamelan A.N., Peucat J.J., Delor C. (1997) - Reliques archéennes (3,15 GA) au sein du magmatisme birimien (2,1 Ga) de Côte d´Ivoire, craton ouest-africain. *C.R. Acad. Sci. Paris*, **324** (IIa), 719-727.

Krogh E.J. (1977) – Origin and metamorphism of iron formation and associated rocks, Lofoten-Vesteralen, N.Norway. *Lithos*, **10**, 243-255.

Krook L., Roever E.W.F. de (1975) - Some aspects of bauxite formation in the Bakhuis Mountains, western Suriname. Anais da Decima Conf. Geol. Interguianas, Belem, Brazil 1, 686-695

Kroonenberg S.B. (1975) - Geology of the Sisa Creek area, SW Suriname. *Geol. Mijnb. Dienst Sur.*, Med. **23**, 103-125.

Kroonenberg S.B. (1976) - Amphibolite-facies and granulite-facies metamorphism in the Coeroeni-Lucie area, southwestern Suriname. Thesis Amsterdam, see also, *Geol. Mijnb. Dienst Sur.*, Med. **25**, 109-289.

Lafon J.M., Rossi P., Delor C., Avelar V.G. de, Faraco M.T.L. (1998) - Novas testemunhas de relíquias arqueanas na crosta continental paleoproterozóica da Província Maroni-Itacaiúnas (Sudeste do Escudo das Guianas). *In*: Cong. Bras. Geol., 40 Belo Horizonte, Anais p. 64.

Lafon J.M., Delor C., Barbosa O.S. (2001) - Granulitos Tardi-Transamazônicos (2,06 Ga) na região norte do Estado do Amapá: o charnoquito de Calçoene. *In*: VII Simpósio de Geologia da Amazônia, Belém, SBG-NO, Resumos Expandidos (CD-ROM).

Lal R.K. (1997) - Internally consistent calibrations for geothermobarometry of high-grade Mg-Al rich rocks in the system $MgO-Al_2O_3-SiO_2$ and their application to sapphirine-spinel granulites of Eastern Ghats, India and Enderby Land, Antarctica. *Proceedings Indian Acad. Sciences* (Earth and Planet. Sci.), **106**, 91-113.

Ludwig K.R. (2001) - User's manual for Isoplot Ex Version 2.49. A geochronological toolkit for Microsoft Excel. Berkeley Geochronology Center, Berkeley, CA, USA, Spec. Pub. no.1a, 59 p.

Montalvão R.M.C., Tassinari C.C.G. (1984) – Geocronologia pré-cambriana do Território Federal do Amapá (Brasil). *In*: II Simposium Amazônico. Manaus, MME/DNPM, Anais, p. 53-57.

Montgomery C.W. (1979) – Uranium-lead geochronology of the Archean Imataca Series, Venezuelan Guyana shield. *Contrib. Mineral. Petrol.*, **69**, 167-176.

Montgomery C.W., Hurley P.M. (1978) - Total rock U-Pb and Rb-Sr systematics in the Imataca Series, Guyana Shield, Venezuela. *Earth Planet. Sci. Lett.*, **39**, 281-290.

Nell J., Wood B.J. (1989) - Thermodynamic properties in a multicomponent solid solution involving cation disorder: $Fe_3O_4-MgFe_2O_4-FeAl_2O_4-MgAl_2O_4$ spinels. *Amer. Mineralogist*, **74**, 1000-1015.

Odon F., Enjolvy R. (2003) - Caractérisation de l'évènement fini-transamazonien. Etude pétrologique des granulites des Monts Bakhuis. Travail d'Etude et de Recherche, Université de Montpellier II, France.

Oliveira E.C., Lafon J.M., Gioia S.M.L., Pimentel M.M. (2002) - Implantação do método Sm-Nd para minerais metamórficos e sua aplicação em rochas da região central do Amapá, Sudeste do Escudo das Guianas. *In*: Congresso Brasileiro de Geologia, 41. João Pessoa - PB. SBG. Anais de resumos. p. 502.

Perchuk L., Gerya T., Nozkhin A. (1989) - Petrology and retrograde P-T path in granulites of the Kanskaya formation, Yenisey range, eastern Siberia. *J. Metamorph. Geol.*, **7**, 599-617.

Pommier A., Cocherie A., Legendre O. (2003) - "EPMA dating": a program for age calculation from electron microprobe measurements of U-Th-Pb. EGS-AGU-EUG. Nice, France, 6-11 April 2003.

Powell R., Sandiford M. (1988) - Sapphirine and spinel phase relationships in the system $FeO-MgO-Al_2O_3-SiO_2-TiO_2-O_2$ in the presence of quartz and hypersthene. *Contrib. Mineral. Petrol.*, **98**, 64-71.

Priem H.N.A., Boelrijk N.A.I.M., Hebeda E.H, Verdurmen E.A.Th., Verschure R.H. (1971) - Isotopic ages of the Trans-Amazonian acidic magmatism and the Nickerie Metamorphic Episode in the Precambrian basement of Suriname, South America. *Geol. Soc. Amer. Bull.*, **82**, 1667-1680.

Priem H.N.A., Boelrijk N.A.I.M., Hebeda E.H, Kroonenberg S.B., Verdurmen E.A.Th., Verschure R.H. (1977) - Isotopic ages in the high-grade metamorphic Coeroeni Group, SW Suriname. *Geol. Mijnbouw*, **56**, 155-160.

Priem H.N.A., Boelrijk N.A.I.M., Hebeda E.H., Kuyper R.P., Roever E.W.F. de, Verdurmen E.A.Th., Verschure R.H., Wilens J.B. (1978) - How old are the supposedly Archean charnockitic granulites in the Guyana Shield basement of western Suriname (South America)? USGS Open File Rept. 78-701, 341-343.

Raith M., Karmakar S., Brown M. (1997) - Ultra-high temperature metamorphism and multistage decompressional evolution of sapphirine granulites from the Palni Hill ranges, southern India. *J. Metamorph. Geol.*, **15**, 379-400.

Ricci P.S.F., Carvalho J.M.A., Rosa-Costa L.T., Lafon J.M. (2002) - Plúton charnoenderbítico Arqueano intrusivo nos ortognaisses granulíticos do Cinturão Jari - Terreno Arqueano expressivo do sudeste do Escudo das Guianas. *In*: Congresso Brasileiro de Geologia, 41. João Pessoa, SBG-NE, Anais, p. 524.

Roever E.W.F. de (1973) - A provisional lithologic framework of the Falawatra Group. Mem. Secondo Congreso Latino-Americano de Geologia, Caracas, 1973. See Bol. De Geologia Publ. Esp. 7.2, 637-948 (1976). Also, *Geol. Mijnb. Dienst Sur.*, Med. **23**, 34-45.

Roever E.W.F. de (1975) - Geology of the central part of the Bakhuis mountains (W Suriname). *Geol. Mijnb. Dienst Sur.*, Med. **23**, 65-101.

Roever E.W.F. de, Kieft C., Murray E.E., Klein E., Drucker W.H. (1976) - Surinamite, a new Mg-Al silicate from the Bakhuis Mountains, W Suriname. *Amer. Mineralogist*, **61**, 193-199.

Rosa-Costa L.T., Ricci P.S.F., Lafon J.M., Vasquez M.L., Carvalho J.M.A., Klein E.L., Macambira E.M.B. (2003) - Geology and geochronology of Archean and Paleoproterozoic domains of southwestern Amapá and northwestern Pará, Brazil, southeastern Guiana Shield. *Géologie de la France*, **2-3-4**, 101-120.

Sandiford M., Neall F.B., Powell R. (1987) - Metamorphic evolution of aluminous granulites from Labwor Hills, Uganda. *Contrib. Mineral. Petrol.*, **95**, 217-225.

Santos J.O.S., Hartmann L.A, Gaudette H.E., Groves D.I., McNaughton N.J., Fletcher I.R. (2000) – A new understanding of the provinces of the Amazon Craton based on integration of field mapping and U-Pb and Sm-Nd geochronology. *Gondwana Res.*, **3**(4), 453-488.

Santos J.O.S., Potter P.E., Reis N.J., Hartmann L.A., Fletcher I.R., McNaughton N.J. (2003) - Age, source and regional stratigraphy of the Roraima Supergroup and Roraima- like outliers in northern South America based on U-Pb geochronology. *Geol. Soc. Amer. Bull.*, **115**, 331-348.

Shaw R.K., Arima M. (1998) - A corundum-quartz assemblage from the Eastern Ghats Granulite belt, India: evidence for high P-T metamorphism? *J. Metamorph. Geol.*, **16**, 189-196.

Snelling N.J., McConnell R.B. (1969) - The geochronology of Guyana. *Geol. Mijnbouw*, **48**, 201-213.

Spooner C.M., Berrange J.P., Fairbairn H.W. (1971) - Rb-Sr whole-rock age of the Kanuku complex, Guyana. *Bull. Geol. Soc. Amer.*, **82**, 207-210.

Stacey J.S., Kramers J.D. (1975) - Approximation of terrestrial lead isotopic evolution by a two stage model. *Earth Planet. Sci. Lett.*, **26**, 207-221.

Suzuki K., Adachi M. (1991) - Precambrian provenance and Silurian metamorphism of the Tsubonosawa paragneiss in the South Kitakami terrane, Northeast Japan, revealed by the chemical Th-U-total Pb isochron ages of monazite, zircon and xenotime. *Geochem. J.*, **25**, 357-376.

Swapp S.M., Onstott T.C. (1989) - P-T-time characterization of the Trans-Amazonian orogeny in the Imataca Complex, Venezuela. *Precambrian. Res.*, **42**, 293-314.

Tassinari C.C.G. (1996) - O mapa geocronológico do craton amazônico no Brasil: revisão dos dados isotópicos. Tese de Livre-docência, Universidade de São Paulo. 139 p.

Tassinari C.C.G., Macambira M.J.B. (1999) - Geochronological Provinces of the Amazonian Craton. *Episodes*, **22(3)**, 174-182.

Tassinari C.C.G., Bettencourt J.S., Geraldes M.C., Macambira M.J.B., Lafon J.M. (2000) - The Amazonian Craton. *In*: Cordani, U.G., Milani E.J., Thomaz Filho A., Campos D.A. (eds.), Tectonic Evolution of South America. 31st Int. Geological Congress, 2000, 41-96.

Tassinari C.C.G., Teixeira W., Nutman A.P., Szabó G.A., Mondin M., Sato K. (2001) - Archean crustal evolution of the Imataca Complex, Amazonian Craton: Sm-Nd, Rb-Sr e U-Pb (SHRIMP) evidences. *In*: Simpósio de Geologia da Amazônia, 7. Belém. (CD-ROM).

Teixeira W., Tassinari C.C.G., Szabó G.J., Mondin M., Sato K., Santos A.P., Siso C.S. (1999) - Sm-Nd Constrains on protolith age of the Archean Imataca Complex, Venezuela. II South American Symposium on Isotope Geology, Actas, 136-138.

Turnock A.C., Eugster A.P. (1962) - Fe-Al oxides: phase relationships below 1000°C. *J. Petrol.*, **3**, 535-565.

Waters D.J. (1991) - Hercynite-quartz granulites : phase relations, and implications for crustal processes. *Eur. J. Mineral.*, **3**, 367-386.

Appendix

Note 1. The nomenclature of the charnockite suite has been used because a) the banded rocks have a close textural resemblance to charnockite, and b) they also contain magmatic components in the form of orthopyroxene-bearing leucosomes (de Roever, 1973, 1975).

Note 2. Orthopyroxene in pelitic gneiss VG 117, VG 101 and WV 257 had been analysed before, but without searching for the highest Al contents in the core of the crystals. Preliminary analysis of orthopyroxene in VG 101 shows up to 8.8% Al_2O_3 in the core.

Note 3. Analyses of sapphirine from VG 117 (Table 2) show a rather low total, around 99%. Re-analysis of sapphirine grains in VG 117 at BRGM yielded similar relatively low totals. ZnO and Cr_2O_3 were also analysed for sapphirines from this sample, but found to be $0 – 0.2\%$ and $0 – 0.1\%$, respectively.